VARIATIONS IN RADIATION RESPONSE DUE TO HYDROGEN: MECHANISMS OF INTERFACE TRAP BUILDUP AND ANNEALING

By

David Russell Hughart

Dissertation

Submitted to the Faculty of the

Graduate School of Vanderbilt University

in partial fulfillment of the requirements

for the degree of

DOCTOR OF PHILOSOPHY

in

Electrical Engineering

December, 2012

Nashville, Tennessee

Approved:

Professor Ronald D. Schrimpf

Professor Daniel M. Fleetwood

Professor Kenneth F. Galloway

Professor Robert A. Reed

Professor Sokrates T. Pantelides

ACKNOWLEDGEMENTS

I would like to thank my advisor, Professor Ronald D. Schrimpf, for his guidance and support. He has always been available to offer advice on many topics, from device physics to presentation pointers. I am grateful for such personal attention and these interactions have made all the years of research meetings enjoyable as well as enlightening.

I would also like to thank Professor Daniel M. Fleetwood for his close involvement in my research. He has taught me a great deal and constantly provided helpful feedback and guidance on my papers and presentations. Both he and Professor Schrimpf have devoted many hours to reviewing my work even when it is submitted late at night, on a weekend, or both. I am very thankful for their patience and their commitment to their students. Their extensive knowledge and passion for research continue to inspire me.

Professor Blair R. Tuttle performed the density functional theory calculations that supported these investigations and has spent many hours discussing and explaining the physics involved, even remotely over video chat. I am very thankful to have had such a great collaborator. I would like to Professor Sokrates T. Pantelides for his help in understanding and interpreting the DFT calculations. I would also like to thank Professor Kenneth F. Galloway and Professor Robert A. Reed for being on my committee.

The numerical simulations were performed using scripts written by Nicole L. Rowsey. I am grateful to her for sharing her work and to Professor Mark E. Law for giving me access to the Florida Object Oriented Device Simulator to perform the simulations for this research.

I would like to thank the U.S. Air Force HiREV program, the Air Force Office of Scientific Research MURI program, the Defense Threat Reduction Agency, and the U.S. Navy for their support of this research.

I am extremely grateful to my friends in the Radiation Effects and Reliability group. They have supported me as both colleagues and friends. Sarah, Jon, and Vishwa have always been the voices of experience and calm and I am indebted to them for their counsel whenever I felt overwhelmed. I have been very lucky to have Nick as a friend, especially one that can stand living with me for four years. Stephanie, Ashley, Cher, Nadia, and Farah have kept me sane when preparing for countless research meetings. I have always been able to count on Sandeepan and Tania for in-depth discussions, both technical and personal, and I thank them for always keeping my spirits high. I would also like to thank Nick, Mike, Nelson, Ray, Daniel, Matt, Pierre, Beth, Michele, Sri, Enxia, Geoff, Nathaniel, Karen, and Paula. It has been a pleasure to spend my graduate school years with such people.

Finally, I would like to thank my parents, for always encouraging and supporting me in whatever I do. They have put up with my busy schedule (resulting in many missed holidays) and my frustrations and disappointments. In response they have always reminded me of how much they care through many phone calls and cards. Thank you for your unconditional love at all times.

TABLE OF CONTENTS

Page

ACKNOWLEDGEMENTS ii

LIST OF FIGURES vi

Chapter

I. INTRODUCTION 1

Overview 2
Organization 3

II. INTERFACE TRAP FORMATION 5

Interface Trap Creation 5
ELDRS 7
Excess Base Current in Bipolar Transistors 10
E' Centers 12
Hydrogen Enhanced Degradation 12
Modeling H_2 Interactions 15
Density Functional Theory Calculations 17
Elevated Temperature Irradiation (ETI) 18

III. HYDROGEN INTERACTIONS WITH COMMON OXIDE DEFECTS 20

Oxygen Vacancy Formation 20
Hydrogen Reactions at V_o Defects 21
Proton Generation at High and Low Levels of Molecular Hydrogen 26

IV. PROTON LOSS AT ELEVATED TEMPERATURES – ANALYTICAL MODEL 31

Experimental Observations 31
Proton Generation and Trapping 33
Reaction Rates 34
Competing Reactions at Elevated Temperatures 38

V. INTERFACE TRAP BUILDUP AND ANNEALING AT ELEVATED

TEMPERATURES– NUMERICAL MODEL 43

Model Details 44
Varying H_2 Concentration..47
Comparison to Experimental Data 48
Contributions of Proton Loss Reactions 49
Variations in Defect Concentration 51
Varying H_2 Concentration and Temperature 53
Elevated Temperature Irradiation Testing 56
Schematic Illustration 61

V. SUMMARY AND CONCLUSIONS 64

REFERENCES 68

LIST OF FIGURES

Figure		Page
2.1	Schematic diagram of charge carrier generation, transport and interactions within SiO_2. After [15].	7
2.2	Relative damage (enhancement factor) versus dose rate for several different bipolar ICs [7].	8
2.3	Interface-trap concentration versus dose rate for lateral *pnp* bipolar transistors irradiated to 30 krad(Si) in three different concentrations of molecular hydrogen [19].	10
2.4	Sc Cross section of a lateral *pnp* bipolar transistor showing the radiation-induced interface traps acting as recombination centers at the surface of the transistor where the current is flowing when biased in forward active mode. After [23].	11
2.5	Plot of output current versus dose for AD590 transducers in packages containing small concentrations of hydrogen and packages with no detectable level of hydrogen [3].	14
2.6	Radiation-induced interface traps and oxide trapped charge versus molecular hydrogen concentration in the field oxide for GLPNP transistors irradiated to 30 krad(SiO_2) [4]	15
3.1	Relative formation energy of oxygen vacancies versus Si-Si bond length [11].	21
3.2	Reaction energies for the dissociation of H_2 at a positively charged oxygen vacancy in the dimer configuration [11]. Points A, B, C, and D are referred to in the text.	23
3.3	Reaction energies for the dissociation of H_2 at a positively charged oxygen vacancy in the puckered configuration [11]	24
3.4	(A) An H_2 molecule near a $V_{o\gamma}^{+}$ defect. In (B) the H_2 has split into a Si-H bond and an $O\text{-}H^{+}$ bond [11].	25
3.5	Reaction energies for the dissociation of H_2 at a neutral oxygen vacancy to create a doubly hydrogenated vacancy [11].	27
3.6	Simulation results compared to experimental data from [4] showing interface-trap buildup as a function of molecular hydrogen concentration [43].	29

3.7 Simulation results compared to experimental data from [19] showing interface-trap buildup as a function of dose rate for three different concentrations of molecular hydrogen concentration [43]. 30

4.1 Excess base current for a lateral PNP transistor as a function of total dose for seven different irradiation temperatures [1]. 32

4.2 Excess base current for a lateral PNP transistor as a function of irradiation temperature for six different total doses [1]. 33

4.3 View of the oxide showing the relative concentrations of protons and VH defects in the oxide. 37

4.4 Value of the diffusivity for protons and holes as a function of temperature. 41

4.5 Value of the reaction rate coefficient for proton release and hydrogen dimerization as a function of temperature. 42

5.1 Simulated interface-trap buildup versus temperature for varying concentrations of H_2 in the oxide. The H_2 levels assumed in the calculations range from 5×10^{13} cm^{-3} to 5×10^{21} cm^{-3}. The total dose is 40 krad(SiO_2). 48

5.2 Simulated interface-trap buildup versus temperature for total doses of 10, 20, and 40 krad(SiO_2) at 294 rad/s, with excess base current plotted on the second y-axis for measurements reported in [1] with the same dose rate and total doses. The H_2 concentration in the simulation is 5×10^{17} cm^{-3}. 49

5.3 Simulated interface-trap buildup versus temperature with proton capture at $V_{o\delta}$ defects suppressed (dashed blue), defect-mediated dimerization at $V_{\delta}H$ defects suppressed (dashed red line), and with normal reactions (solid black line) with the H_2 concentration at 5×10^{17} cm^{-3} 50

5.4 Simulated interface-trap buildup versus temperature with an order of magnitude increase or decrease in $V_{o\delta}$ defects and $V_{o\gamma}$ defects with the H_2 concentration at 5×10^{17} cm^{-3}. 52

5.5 Simulated interface-trap buildup versus temperature for an order of magnitude increase in $V_{\delta}H_2$ defects and an order of magnitude decrease in $V_{o\delta}$ defects with the H_2 concentration at 5×10^{13} cm^{-3}. 53

5.6 Simulated interface-trap buildup versus temperature with proton capture at $V_{o\delta}$ defects suppressed (dashed blue line), defect-mediated dimerization at $V_{\delta}H$ defects suppressed (dashed red line), and with normal reactions (solid black line) with the H_2 concentration at 5×10^{21} cm^{-3} 56

5.7 Excess base current vs. temperature for pnp transistors irradiated with all terminals grounded at 294 rad/s at 10 krad(SiO_2) and 20 krad(SiO_2) with the room temperature results for a dose rate of 0.001 rad/s marked on the graph [1]. 58

5.8 Simulated interface-trap buildup vs. temperature at 294 rad/s and 0.001 rad/s at 20 krad(SiO_2). The H_2 concentration is 5×10^{17} cm^{-3}. 59

5.9 Simulated interface-trap buildup vs. time after irradiation at 294 rad/s and 478 K with a H_2 concentration of 5×10^{21} cm^{-3}. 60

5.10 Proton transport and interactions at or near the interface for room temperature and elevated temperature. H^+ is a proton, VH is a hydrogenated oxygen vacancy, VH_2 is a doubly hydrogenated oxygen vacancy, $V_{o\delta}$ is a dimer precursor oxygen vacancy, $V_{o\gamma}$ is a puckered precursor oxygen vacancy, O is a Si-H bond, X is an interface trap, and the size of the arrows are a rough approximation of the magnitudes of the reaction rate or speed of transport. (a) Oxide conditions at room temperature. (b) Oxide conditions at moderate temperature. (c) Oxide conditions at elevated temperatures...63

CHAPTER I

INTRODUCTION

Radiation-induced interface traps are among the primary reliability concerns for electronics in space. Extensive research has been done to understand the mechanisms responsible for their creation and passivation. Experiments have documented the creation of interface traps in both MOS and bipolar technologies under many conditions, including varying temperatures [1], [2], ambient hydrogen concentrations [3]-[5], processing conditions [6], and dose rates [7]. Identifying and understanding the effects of the various conditions are critical for predicting how electronics will behave. Many examples of this can be seen in the current literature. One of the primary examples is Enhanced Low Dose Rate Sensitivity (ELDRS). ELDRS is a phenomenon where certain parts, typically bipolar junction transistors, experience higher degradation at low dose rates than at high dose rates [7]. This discovery prompted concerns about the radiation testing done on Earth, which generally uses very high dose rates compared to what electronics are exposed to in space. Understanding and predicting this enhanced degradation are still ongoing topics of research [8]-[10]. Hydrogen plays a key role in interface-trap formation and annealing and learning how it behaves is central to understanding radiation response. The incorporation [11], introduction [4], transport [12], and reactions [11], [13] of hydrogenous species in the oxide have been modeled to provide insight into the mechanisms that lead to the buildup and annealing of radiation-induced interface traps. These range from the two-stage model [14], [15] to explain basic

interface-trap formation, to more complex models involving competition between electron-hole recombination and hydrogen release [16], [17] to explain dose rate effects.

Previous experiments investigating elevated temperature irradiation (ETI) have shown both enhanced degradation and annealing effects, depending on the irradiation temperature, dose rate, and total dose [1]. Recent first principles physics calculations have provided significant insight into the reactions that can occur at some common defects in oxides [11]. Proton release mechanisms and defect interactions under a variety of conditions are identified that provide insight into enhanced degradation in the presence of molecular hydrogen, irradiation at elevated temperatures, and dose rate effects. The results demonstrate how proton loss reactions can limit the supply of protons at the interface and suppress interface-trap buildup at elevated temperature [18].

Overview

Hydrogen produces variability in the radiation response of integrated circuits, whether incorporated in the oxide or present in the surrounding environment as a gas. The presence of molecular hydrogen can increase interface-trap buildup [4] and alter dose rate response [19]. Defects with hydrogen incorporated in the oxide during processing can suppress interface-trap buildup at elevated temperatures [18]. This thesis explores the reactions of hydrogenous species at common oxide defects and the mechanisms that explain radiation-induced interface-trap formation and annealing, focusing on the effects of temperature, molecular hydrogen concentration, and dose rate. Density functional theory (DFT) calculations [11] that identify defects likely to be present in common thermal oxides and provide energy barriers for reactions at those defects are presented

and important mechanisms for interface-trap buildup and annealing are extracted and discussed. These mechanisms are implemented in a numerical model that simulates interface-trap buildup in a 1-D slice of oxide and silicon using the estimates for defect concentrations and energy barriers from the DFT calculations. The results provide insight into which reactions have a significant impact on interface-trap density under a variety of conditions; the predictions are compared to experimental data.

Organization

This rest of the thesis investigates the physical processes responsible for interface-trap buildup and annealing and how they are affected by various environmental conditions.

Chapter II provides background on interface-trap creation. The defects and reactions involved are presented, along with experimental observations on how dose rate, temperature, and H_2 affect interface-trap buildup and annealing. Previous modeling efforts and mechanisms are discussed. Chapter III goes into greater detail about the nature of the defects present in the oxide and the energetics of the reactions that occur there. Mechanisms for interface-trap creation are presented based on first principles physics calculations. Chapter IV takes the energy barriers provided by these calculations and provides an analytical comparison of reactions at elevated temperatures that demonstrates how reactions that remove protons from the oxide can become favorable, limiting interface-trap buildup. Chapter V presents numerical simulations that implement a detailed set of reactions at every defect considered in the physics calculations presented in Chapter III. The results produce data similar to experimental observations and provide

a more physical understanding of how interface-trap buildup is affected by temperature, dose rate, and molecular hydrogen concentration. Chapter VI concludes the thesis, summarizing the key results and highlighting the advances in understanding. The implications of these results are discussed.

CHAPTER II

INTERFACE TRAP FORMATION

Holes created by ionizing radiation may release hydrogen in the form of protons that can transport to the interface and depassivate Si-H bonds, creating interface traps [15]. This process depends on various defects in the oxide that facilitate hole transport and act as reaction sites, as well as the various mobile species that are the reactants. Other factors like dose rate, temperature, and molecular hydrogen concentration affect the buildup and annealing of interface traps as well. Numerous experiments have been performed and models created to investigate the defects and mobile species involved in these processes. This chapter discusses how interface traps are formed, their effects, and how their formation can be affected by other factors. The basic reactions and reactants responsible for interface-trap formation are identified. Experimental observations of the effects of dose rate, temperature, and H_2 concentration are discussed, as well as some approaches used to simulate interface-trap formation.

Interface Trap Creation

The mechanisms responsible for interface-trap creation have been extensively studied. The consensus is that the dominant process is the depassivation of Si-H bonds at the interface by protons released by holes generated by ionizing radiation [15]. Radiation generates electron-hole pairs in the oxide. Fig. 2.1 depicts the transport and trapping reactions for electrons and holes in a MOS structure under positive bias. Electrons are

transported toward the gate while holes are transported toward the interface. For bipolar devices, the overall picture is similar, but without a gate providing positive bias, the electric field is largely determined by work function differences and is much lower. This results in lower charge yields since the electric field helps to separate holes and electrons created by ionizing radiation before they recombine [15]. The low electric field also means that the primary charge transport mechanism is diffusion instead of drift and that there is increased chance that electrons can neutralize trapped holes before they can release protons [17]. Additionally, space charge has a larger effect on the local fields and can affect charge transport [20], [21]. Note that interface-trap buildup also occurs with negative electric fields present and is likely due to hydrogen sources in the bulk silicon [22]. This thesis primarily focuses on the low electric field case and considers how hydrogen interactions in the oxide can affect radiation-induced interface-trap buildup. The radiation-induced degradation depends on the hole yield, the number of holes that escape recombination with electrons, which is determined primarily by the energy of the radiation, the strength of the electric field in the oxide, and the initial concentration of electron hole pairs [15]. Once holes are generated, they rapidly become trapped in shallow traps and migrate via polaron hopping, moving from one trap to the next [15]. While holes are migrating through the oxide, they can interact with defect sites containing hydrogen, releasing the hydrogen as protons H^+ [15], [17]. Protons then are transported to the interface where they can depassivate Si-H bonds, creating interface traps via the following reaction:

$$H^+ + Si\text{-}H \rightarrow Si\text{-}^+ + H_2 \, . \qquad (2.1)$$

Si-+ is a dangling bond that can act as a recombination center, an interface trap.

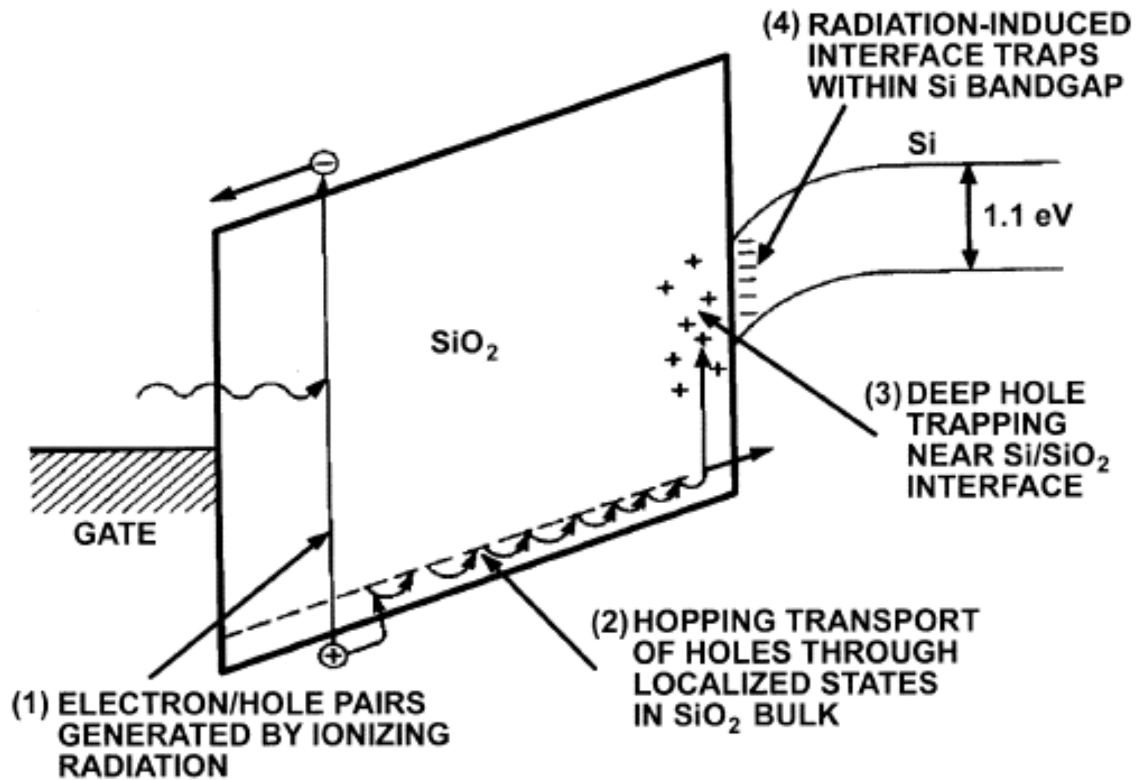

Fig. 2.1. Schematic diagram of charge carrier generation, transport and interactions within SiO_2. After [15].

<u>ELDRS</u>

The irradiation dose rate can have a significant effect on the radiation response of some parts, causing increased degradation at a low dose rate compared to a higher dose rate at the same total dose. Parts that show this increased degradation at low dose rates are considered to exhibit Enhanced Low Dose Rate Sensitivity (ELDRS). ELDRS is a major issue for linear bipolar transistors [23]-[25], especially since dose rates in space are generally much lower than the dose rates used for testing parts on Earth; the search for a general method to screen ELDRS-sensitive parts at higher dose rates is still ongoing.

Note that parts are only considered to exhibit ELDRS if they exhibit a true dose rate effect, such that even if the high dose rate device is annealed at room temperature for the same length of time as the irradiation at low dose rate, the degradation at low dose rate is still greater. The relative increase in degradation from high dose rate plus anneal to low dose rate is called the true dose rate enhancement factor [26]. Fig. 2.2 shows an example of enhancement factors versus dose rate for several types of bipolar ICs.

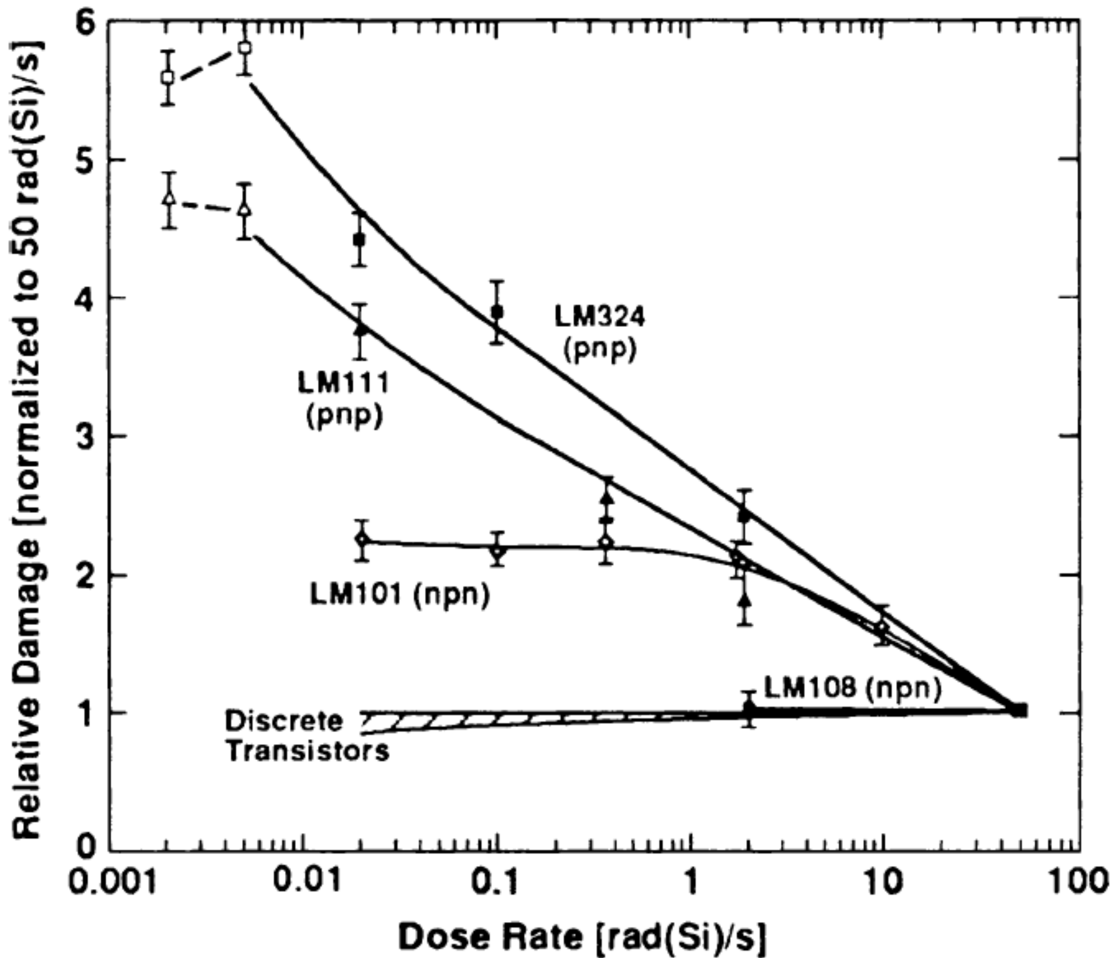

Fig. 2.2. Relative damage (enhancement factor) versus dose rate for several different bipolar ICs [7].

There are many theories to explain why ELDRS occurs. Some of the prominent ones are briefly described here. It has been proposed that the space charge created in the bulk of the oxide affects the transport of other charged species, reducing the number of protons that arrive at the interface [27], [28]. It has also been suggested that the density of defects that act as Shockley-Read-Hall recombination centers compared to the density of defects that act as shallow hole traps is important since an increased availability of recombination centers reduces the holes available to release protons [29]. The presence of hydrogen, which can be released from the packaging [3] or be present in some part of the device like the passivation layers [6], has also been shown to be an important factor in the ELDRS response of bipolar devices [4], [19]. When ionizing radiation creates electron-hole pairs, under positive bias, electrons are transported to the gate and holes are transported to the interface. While migrating toward the interface, holes have a chance to either recombine with electrons or release hydrogen from defects in the form of protons that can migrate to the interface and create interface traps. Once a hole has transferred its charge to a proton, it is unlikely to be neutralized by an electron, making this competition between recombination and proton release key to the amount of degradation [17]. At high dose rates when large concentrations of electrons and holes are present simultaneously, more holes recombine with electrons, limiting the interface traps created by protons [17]. Introducing additional hydrogen increases the number of holes that release protons instead of recombining with electrons, suppressing high dose rate effects and resulting in higher degradation for a given dose rate [17]. Fig. 2.3 plots results from [19] that plot interface-trap density versus dose rate for lateral *pnp* transistors soaked in varying concentrations of hydrogen, showing how the presence of molecular hydrogen during

irradiation not only increases interface-trap buildup, but also causes the dose rate at which the transition between high and low dose rate degradation occurs to shift to higher dose rates. ELDRS effects also depend on a number of other factors such as processing steps, pre-irradiation testing procedures, aging, temperature, and bias [6], [20], [26], [30].

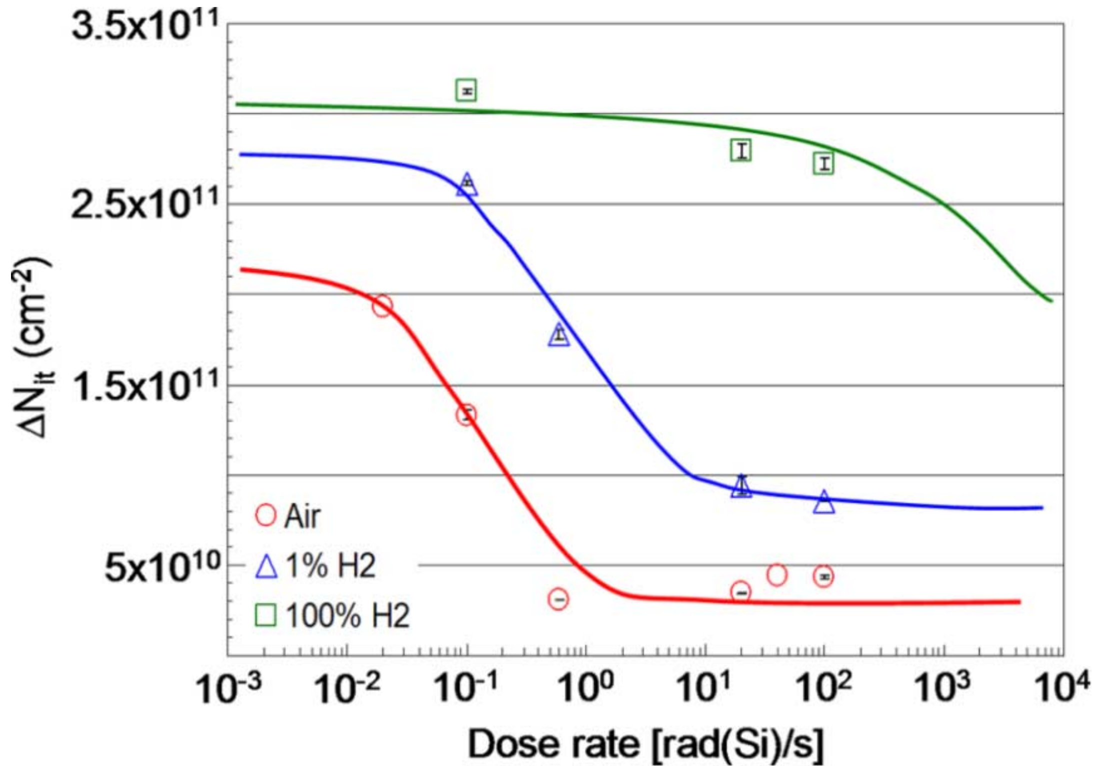

Fig. 2.3. Interface-trap concentration versus dose rate for lateral *pnp* bipolar transistors irradiated to 30 krad(Si) in three different concentrations of molecular hydrogen [19].

<u>Excess Base Current in Bipolar Transistors</u>

It is useful to briefly discuss the effects of radiation-induced interface traps on lateral *pnp* bipolar transistors because of the direct effect they have on excess base current, making lateral *pnp* transistors common devices to provide a measure of interface-trap buildup. The primary effect of total ionizing dose (TID) on lateral PNP bipolar

transistors is gain degradation caused by interface traps [23]. When traps are created at the Si/SiO_2 interface during irradiation, they introduce additional recombination centers in the silicon band gap, resulting in an increase in the surface recombination velocity. The area of concern for a lateral *pnp* transistor is the region over the active base, since the current flow between the emitter and the collector is at the surface of the transistor and is strongly affected by the increased recombination centers, as seen in Fig. 2.4 [23]. The increase in surface recombination causes an increase in the base current. The increase in base current compared to the pre-irradiation value is called the excess base current, which degrades the current gain of the transistor, defined as the ratio of the collector current to the base current. This is a critical parameter since bipolar devices are often used as current amplifiers.

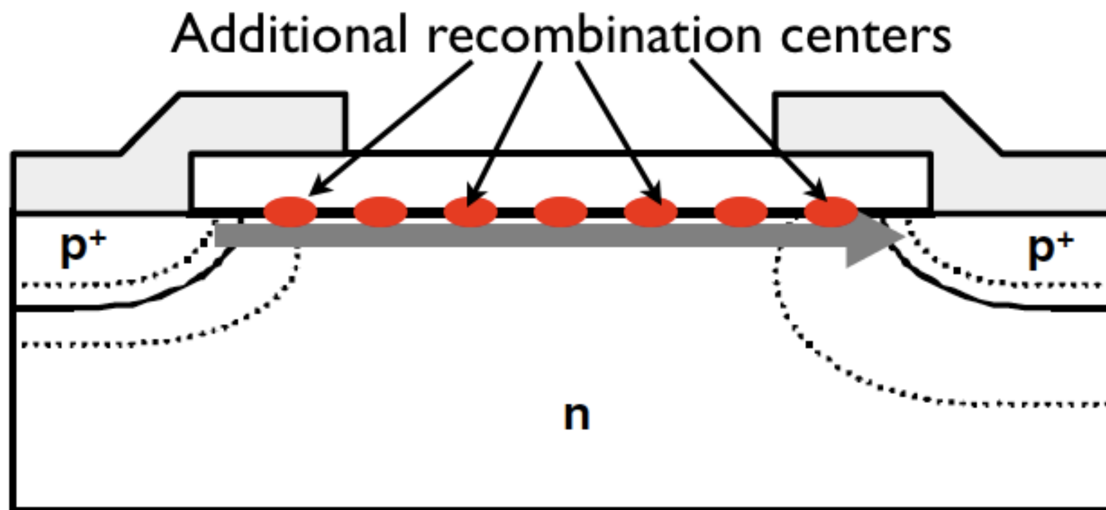

Fig. 2.4. Cross section of a lateral *pnp* bipolar transistor showing the radiation-induced interface traps acting as recombination centers at the surface of the transistor where the current is flowing when biased in forward active mode. After [23].

E' Centers

When holes are created in the oxide, they can be trapped at defects and then either react with another species in the oxide, or detrap from the defect and move to another defect [15]. Numerous studies show that the defects with which holes primarily interact are E' defects [31]-[33], which are most likely oxygen vacancies (V_o) [34]. Experiments [35] and theory [36] indicate that when a vacancy has trapped a hole it assumes either a dimer or puckered configuration. Neutral oxygen vacancies are either dimer precursors ($V_{o\delta}$) or puckered precursors ($V_{o\gamma}$). Due to differences in the defect energy levels, holes remain trapped at defects in the puckered configuration much longer than at defects in the dimer configuration [11], [35]. Dimer precursors are more likely to mediate hole transport, while puckered precursors tend to serve as reaction centers or fixed charge.

Hydrogen Enhanced Degradation

The presence of molecular hydrogen affects interface-trap density. If present near the interface, molecular hydrogen can passivate interface traps, annealing the damage [37]. However, ambient hydrogen enhances the degradation of several types of linear bipolar devices when they are exposed to ionizing radiation [3], [4], [38] indicating that hydrogen is involved with both interface-trap buildup and annealing. In [3] the radiation response of the AD590 temperature transducer varies based on the packaging of the devices. Parts packaged in flat-packs show higher changes in output current, a sign of increased degradation, than parts packaged in TO-52 cans [3], as shown in Fig. 2.5. Residual gas analysis revealed that there was a small concentration of hydrogen present

in the flat-packs, but no detectable hydrogen concentration in the TO-52 cans, suggesting that hydrogen was responsible for the enhanced degradation [3]. In order to understand the relationship between the presence of hydrogen and degraded radiation response of bipolar devices, experiments were performed that soaked bipolar transistors prior to irradiation in either varying concentrations of hydrogen [4] or 100% hydrogen concentration for varying amounts of time [38]. Their radiation responses were then compared at a given total dose. The results showed that, in both cases, the concentration of radiation-induced interface traps and oxide trapped charge increased with the amount of hydrogen present, as seen in Fig. 2.6. One of the mechanisms proposed for hydrogen enhanced degradation is the cracking of H_2 molecules at a charged defect, an E' center [39], [40]. Reactions between H_2 molecules and oxide defects have been explored using first principles physics calculations [38], [41]; however, there was no research on the likelihood of the chosen defects being present in significant quantities in the oxides of the real world devices.

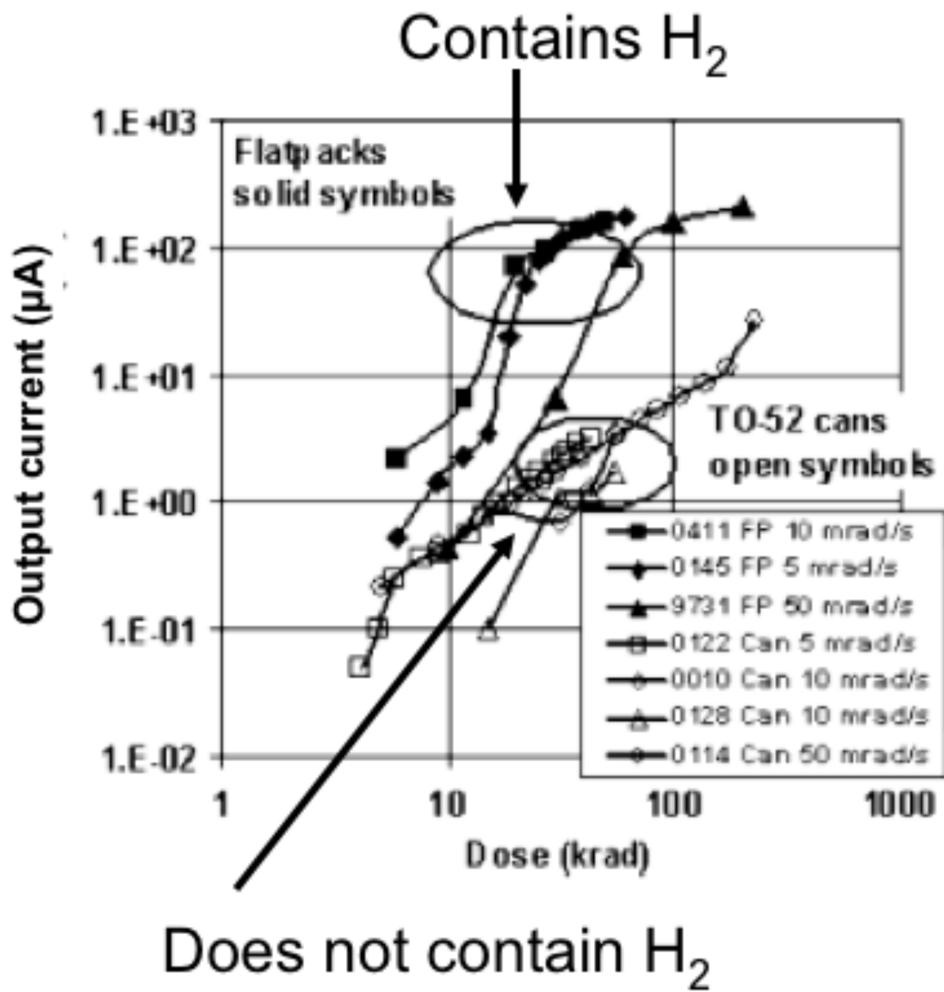

Fig. 2.5. Plot of output current versus dose for AD590 transducers in packages containing small concentrations of hydrogen and packages with no detectable level of hydrogen [3].

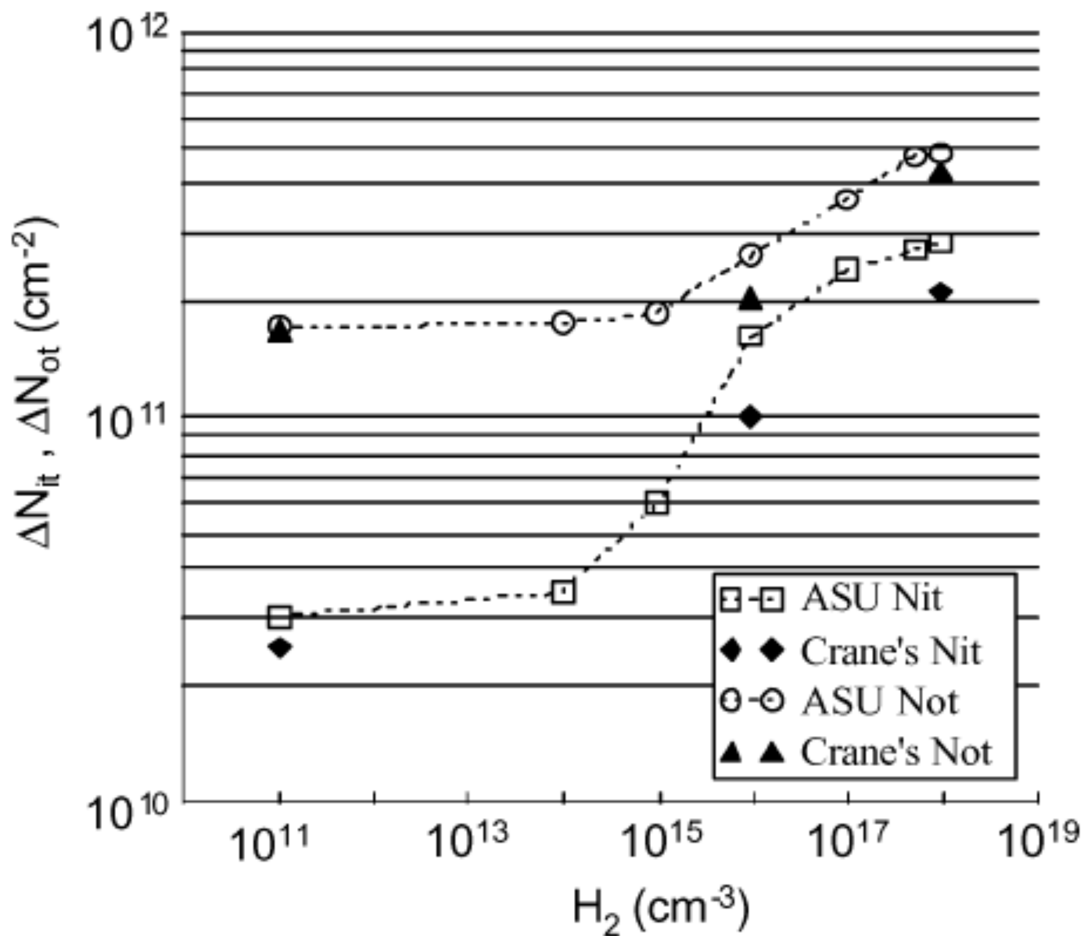

Fig. 2.6. Radiation-induced interface traps and oxide trapped charge versus molecular hydrogen concentration in the field oxide for GLPNP transistors irradiated to 30 krad(SiO_2) [4].

Modeling H_2 Interactions

A variety of reactions involving molecular hydrogen have been modeled to account for effects on interface-trap formation. Most recently, the focus has been on explaining enhanced degradation in the presence of H_2 [4] and dose rate effects [16], [42]. These models generally consist of a set of continuity equations for the species involved that describe generation and recombination and transport via drift and diffusion

and the effect of electric field. There have been a variety of approaches. In [4], Chen et al. use an analytical model to relate hydrogen exposure to enhanced interface-trap formation by suggesting H_2 cracks at a defect in the oxide, creating more potential reaction sites for holes to release protons. This matched the data shown in Fig. 2.6. This model assumes the presence of a processing defect that reacts with H_2 to form defects that release protons in the presence of holes created during irradiation. Batyrev et al. [38] also attempt to explain hydrogen-enhanced degradation, this time numerically simulating a set of reactions that incorporate first principles physics calculations into some of the reaction rate calculations. This model also assumes that H_2 molecules react at neutral defects, presumed to be oxygen vacancies in this paper, and that holes then release protons from the resulting hydrogenated defect. Electrons are assumed to exit the oxide quickly and the effects of recombination are ignored except for the calculation of the initial hole yield during irradiation. Chen et al. [42] simulate the dose rate response by modifying the electron-hole recombination rate directly since it changes as increasing hydrogen concentration creates a competition between recombination and proton release. While including the effects of recombination, no specific reactions are implemented, simply a recombination term representing the effective electron-hole recombination. Again, proton release is considered to be due to a hole reacting at a hydrogenated defect, the concentration of which is adjusted to account for changes in concentration of molecular hydrogen. All of the models presented thus far did not include terms to account for reverse reactions. Hjalmarson et al. [16] simulated dose rate variations differently, describing a set of bimolecular reactions between a number of potential defects and mobile species. Transport parameters are specific to each mobile species. This model

considers both proton release from hydrogenated defects and the dissociation of molecular hydrogen at positively charge defects and accounts for reverse reactions. Reaction rate coefficients are not unique; one value was used for reactions involving uncharged species and a second was used for reactions involving charged species. Rowsey et al. [43] implement reactions based on first principles physics calculations that calculate forward and reverse reaction rates for each reaction. Some reactions are simplified, describing the capture and subsequent release of a mobile species at a defect in one reaction using a single forward and reverse energy barrier. In this thesis a model is presented that calculates forward and reverse reaction rates based on DFT calculations that take intermediate steps in each reaction into account. This allows multiple reaction pathways that can have different energy barriers. Transport parameters and reaction rates are affected by temperature in this model, providing insight into which mechanisms are important at different temperatures.

Density Functional Theory Calculations

The mechanisms of interface-trap buildup and annealing depend on reactions involving hydrogen at various point defects. In order to develop more accurate models, first principles physics calculations are used that describe these reactions at an atomic level. Previously, reactions involving hydrogen have been studied with a variety of theoretical calculations. Estimates of reaction energies were calculated using semi-empirical molecular orbital theory [44]. Next, cluster models of the oxide were used, involving a cluster of atoms to describe a defect based on α-quartz structure. Results for point defects are applied to amorphous silicon dioxide because the local structure does

not depend significantly on long-range order [45]. Later calculations used periodic supercells with α-quartz and amorphous configurations [46]. However, these studies explored a limited number of defects and did not address a comprehensive set of defects that are actually found in device quality oxides.

Elevated Temperature Irradiation (ETI)

Experiments in which bipolar transistors are irradiated at elevated temperatures at moderate to high dose rates show that the gain degradation attributed to interface-trap buildup is enhanced compared to irradiations at room temperature [27], [47], [48]. This is of interest because these bipolar transistors also exhibit ELDRS, showing more interface-trap buildup at a given total dose when the devices are irradiated at low dose rates than at high dose rates [27], [49]. Elevated temperature irradiation was evaluated as a possible test to predict low dose rate degradation at higher dose rates [1], [2], [27], [47], [48]-[50]. The reason that ELDRS testing is of so much concern is because space is a low-dose-rate environment and dose rates commonly used on Earth to test parts are significantly higher. In response to this, parts that may exhibit ELDRS must be tested at a low dose rate or undergo a test designed to accelerate radiation-induced degradation and simulate low-dose-rate effects. Testing at a low dose rate is usually undesirable because such testing may take many months. However, while ELDRS has been documented for more than twenty years, no completely satisfactory accelerated hardness assurance test has been identified.

It is hypothesized that ETI accelerates the movement of charge and mitigates space charge effects that are often observed in linear bipolar devices and integrated

circuits irradiated at high dose rates at room temperature [20], [27]. Experiments show that, while ETI can enhance degradation for ELDRS sensitive parts as compared with room temperature irradiation at a moderate to high dose rate, the lower rate degradation is often significantly greater [2], [48], [51]. Additionally, ETI only enhances degradation up to certain temperatures, above which degradation is reduced instead of enhanced [1], [50]. This reduction is attributed to enhanced annealing at high temperatures [1], [50], but the physical mechanisms of these processes are not well understood. Additionally, it is found that high temperature annealing after irradiation can cause significant recovery, reinforcing that high temperatures can improve the radiation response of devices and involve different mechanisms than ELDRS [52]. These results demonstrated that while ETI irradiation may correctly produce low-dose-rate degradation in some cases, there is significant variability in the radiation response among parts. Thus, understanding the physical mechanisms at work during low dose irradiation and elevated temperature irradiation is important for evaluating the radiation hardness of parts and assessing the effectiveness of accelerated test methods.

CHAPTER III

HYDROGEN INTERACTIONS WITH COMMON OXIDE DEFECTS

In order to determine potential interface-trap formation and annealing mechanisms applicable to real world oxides, first principles physics calculations were performed to determine the most likely defects to be present in device-quality oxides and explore the reactions that occur at those sites [11]. The energetics of hydrogen interactions at a variety of defects are considered. Based on these energies, mechanisms for proton generation from the direct release of a proton at a defect via a hole and the dissociation of molecular hydrogen at positively charged defects are formulated.

Oxygen Vacancy Formation

Oxygen vacancies in silicon dioxide facilitate hydrogen and hole transport and act as reaction sites [34]. Defect interactions are modeled in a cube of silicon dioxide with an edge length of 1.2 nm, a large enough volume to model hydrogen interactions with defects in a bulk oxide [11]. In this model, the oxygen vacancy defects are created by removing an oxygen atom and letting the structure relax, resulting in a stretched Si-Si bond [11]. The formation energy is calculated by comparing the energy of the fully relaxed structure to the normal bulk model with no defects [11]. The formation energies of over one hundred oxygen vacancies have been computed and are found to be correlated with the length of the stretched Si-Si bond [53], [54], as seen in Fig. 3.1. Vacancies with lower formation energy are much more likely to form and are present in

significantly larger quantities than vacancies with higher formation energies [11]. The ten most plentiful oxygen vacancies as determined by this calculation are selected for further study and the energetics of various reactions at these defect sites are investigated.

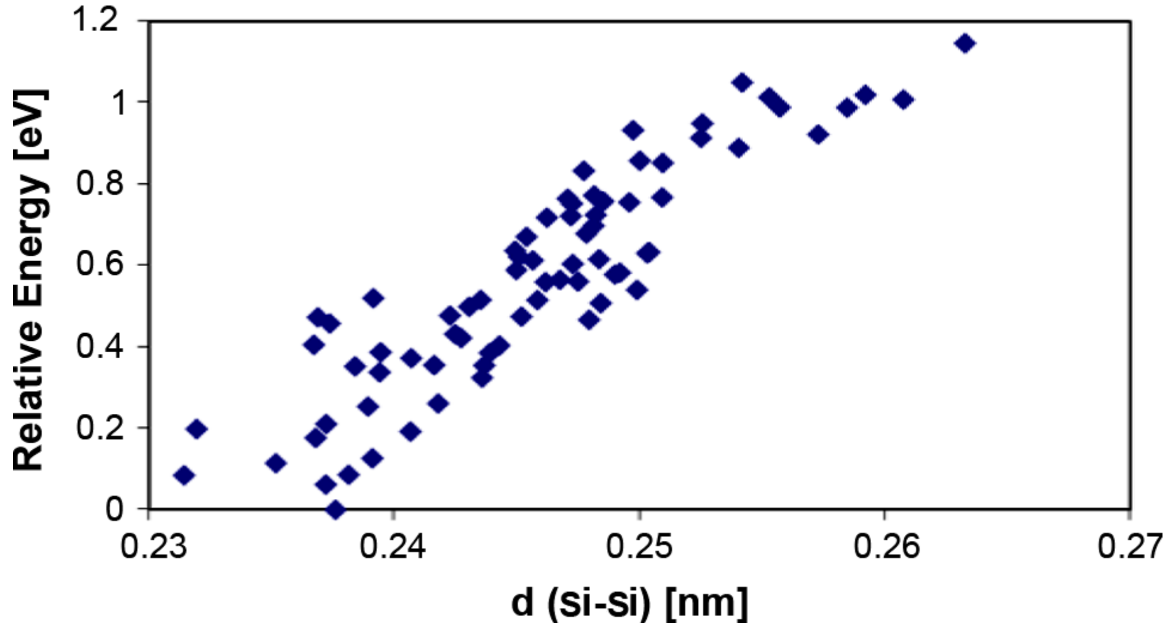

Fig. 3.1. Relative formation energy of oxygen vacancies versus Si-Si bond length [11].

Hydrogen Reactions at V_o Defects

Based on experimental [4], [40], [44] and theoretical [38], [45], [46] work, molecular hydrogen can dissociate, or crack, at charged defects in SiO_2; however, the identification of which oxygen vacancies are most likely to form have not been considered previously. Oxygen vacancies can become charged after irradiation by trapping a hole. As noted previously, charged vacancies assume either a dimer or puckered configuration [36], [55], [56] after trapping a hole via the following reactions:

$$h^+ + V_{o\delta} \rightarrow V_{o\delta}^+ . \quad (3.1)$$

$$h^{+} + V_{o\gamma} \rightarrow V_{o\gamma}^{+} . \quad (3.2)$$

$V_{o\delta}$ and $V_{o\gamma}$ are precursors for the dimer ($V_{o\delta}^{+}$) and puckered ($V_{o\gamma}^{+}$) configurations. The possible reactions of H_2 at both of these defects are considered.

H_2 interactions with the positively charged dimer defect have been studied experimentally with electron paramagnetic resonance (EPR) [57], [58] and theory [59], [60]. The cracking reaction at this defect is:

$$H_2 + V_{o\delta}^{+} \rightarrow VH + H^{+} . \quad (3.3)$$

VH is a hydrogenated vacancy. The energy barrier for this reaction is calculated at each of the ten low-energy oxygen vacancy sites and Fig. 3.2 shows the reaction energetics for the lowest barrier. The reaction occurs in multiple steps. First, the H_2 molecule approaches the vacancy from a minimum energy point (now at point A), then forms two Si-H bonds at the vacancy (point B), and finally one of the bonds breaks, releasing a proton that can transport away along the network oxygen atoms (points C and D) [11]. When factoring in the energy of the neighboring oxygen atoms that the proton hops along using the proton diffusion barrier [61], the overall barrier for proton release from this defect is ~1.4 eV to ~1.7 eV [11]. The energy of structure with the proton diffusing away from the defect is higher than the initial structure, making the reverse reaction favorable. Protons are more likely to be trapped instead of generated via reaction (3.3).

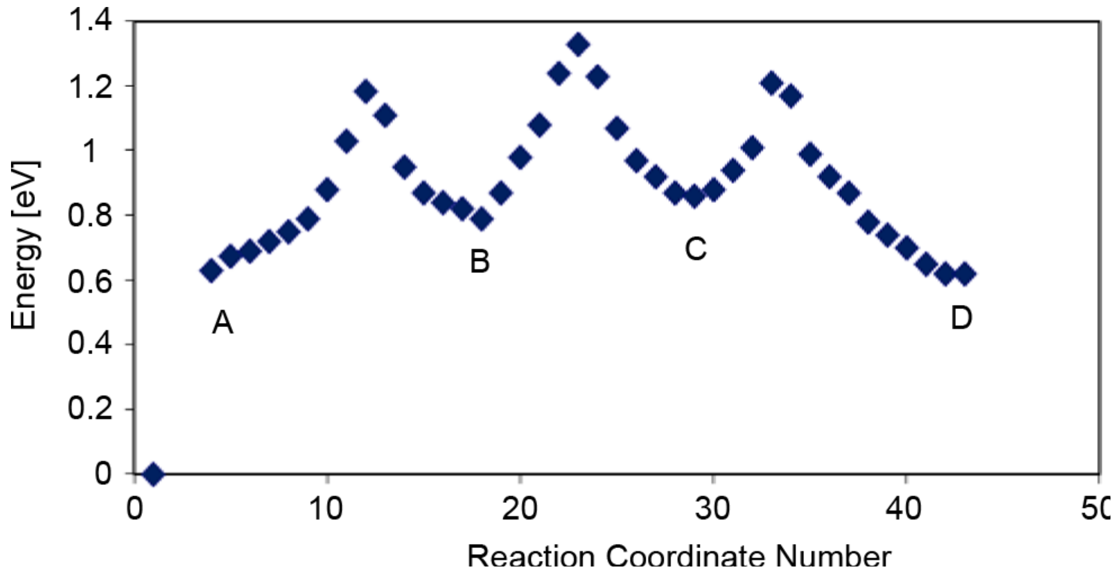

Fig. 3.2. Reaction energies for the dissociation of H_2 at a positively charged oxygen vacancy in the dimer configuration [11]. Points A, B, C, and D are referred to in the text.

The cracking of H_2 at positively charged oxygen vacancies in the puckered configuration is also considered. The concentration of these defects is believed to be roughly an order of magnitude lower than $V_{o\delta}$ defects [53], [54], [55] and two out of the ten vacancies selected for these calculations form a puckered defect [11], results similar to the literature. The cracking reaction at this defect is:

$$H_2 + V_{o\gamma}^{+} \rightarrow VH + H^{+} . \qquad (3.4)$$

The reaction energies for cracking of H_2 at a $V_{o\gamma}^{+}$ defect are shown in Fig. 3.3. The energy for the proton diffusing away is lower than the initial energy and the forward reaction is favored, releasing protons at $V_{o\gamma}^{+}$ defects. Fig. 3.4 shows the initial and final states of the reaction. In Fig. 3.4(a) an H_2 molecule is shown in the vicinity of a puckered oxygen vacancy and in Fig. 3.4(b) the H_2 molecule has dissociated and one hydrogen is bonded to the silicon atom, producing an Si-H bond and the other hydrogen atom has a positive charge and is bonded to an oxygen atom. This is a proton, free to transport away.

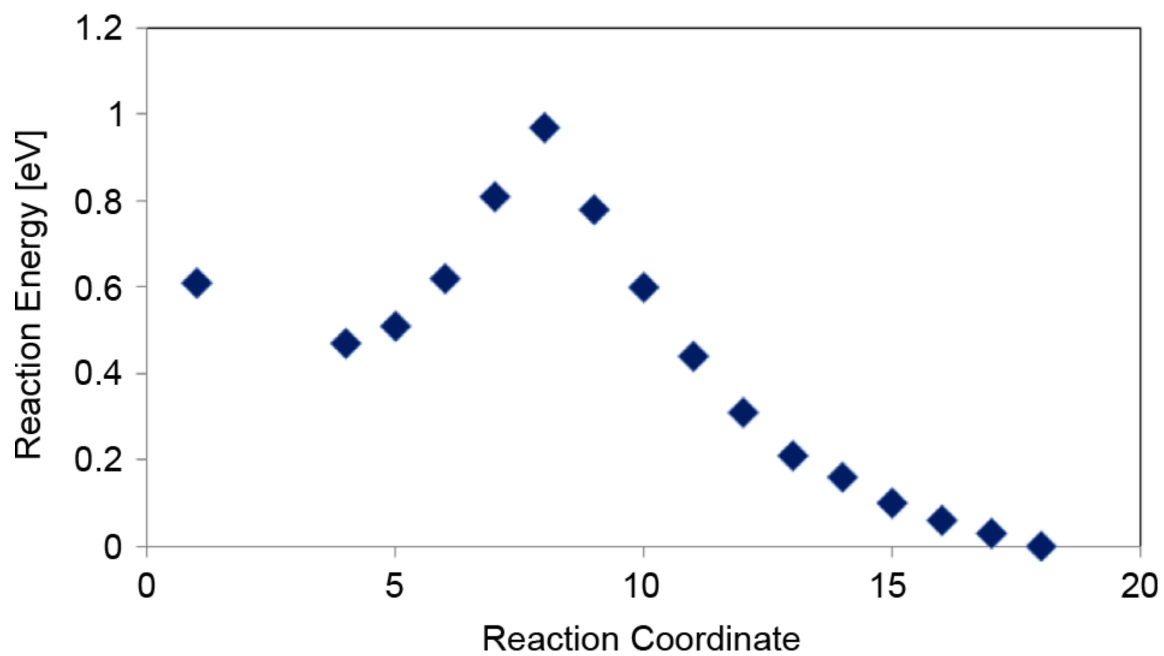

Fig. 3.3. Reaction energies for the dissociation of H_2 at a positively charged oxygen vacancy in the puckered configuration [11].

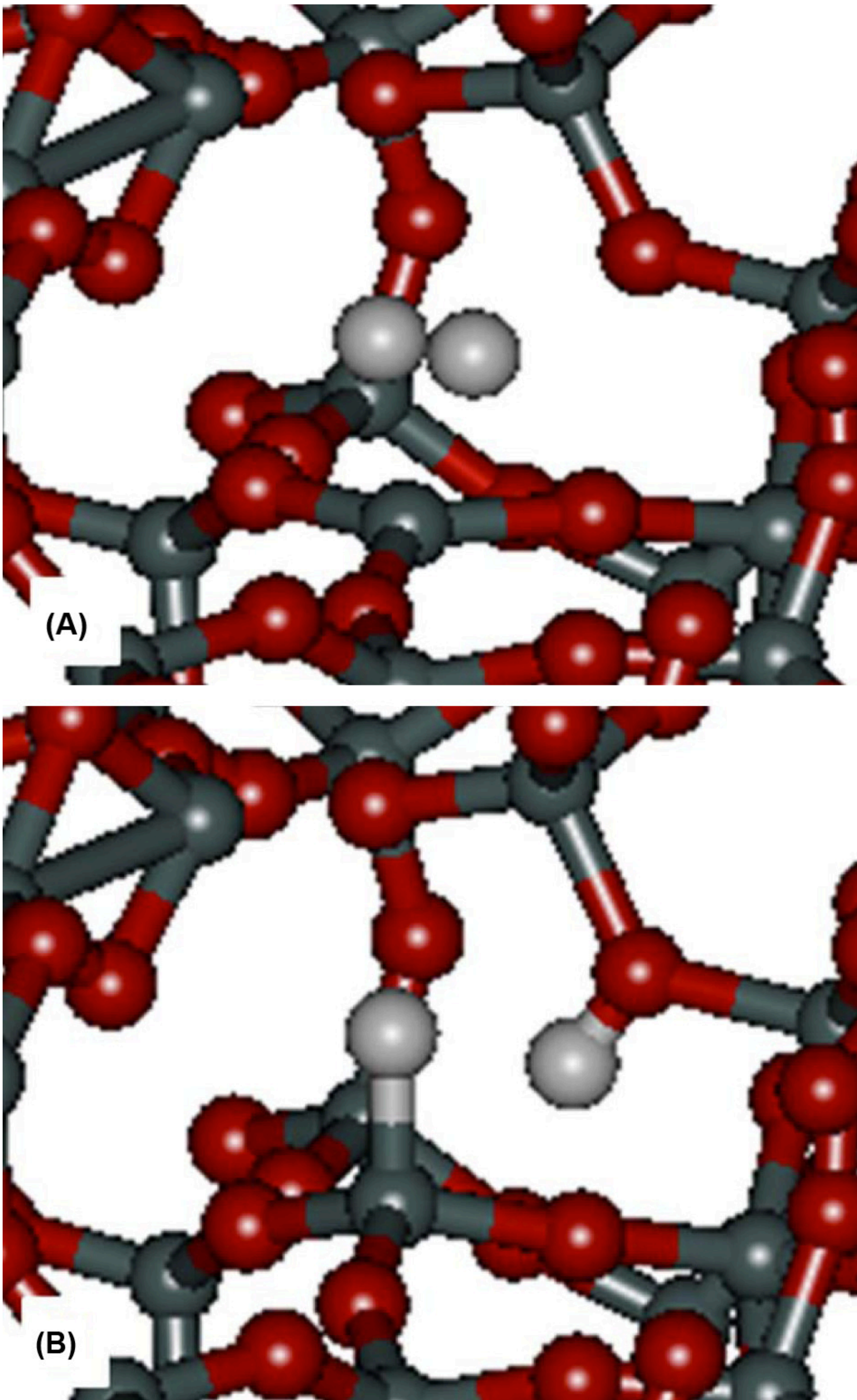

Fig. 3.4. (A) An H_2 molecule near a $V_{o\gamma}^{+}$ defect. In (B) the H_2 has split into a Si-H bond and an $O\text{-}H^+$ bond [11].

Proton Generation at High and Low Concentrations of Molecular Hydrogen

The reaction energies calculated in [11] are implemented in a 1-D model of silicon dioxide and silicon to study the proton generation caused by the various reactions under investigation. These simulations are performed using a simplified version of the model described in greater detail later. The cracking of H_2 at $V_{o_\gamma}^+$ defects produce a significant concentration of protons at high concentrations of H_2, helping to explain the increase in interface-trap buildup seen in Fig. 2.6. In the absence of excess H_2 in the oxide, radiation still produces interface traps. For this case, the release of protons via holes from hydrogenated defects is considered.

Holes can interact with hydrogenated vacancies in the oxide and release hydrogen as protons. Initially, singly hydrogenated vacancies were considered due to the low energy barrier for proton release, ~0.4 eV. This occurs via the following reaction:

$$h^+ + VH \rightarrow V_o + H^+ . \qquad (3.5)$$

However, the concentration of VH defects is roughly two orders of magnitude lower than that of dimer oxygen vacancy precursors, and this reaction does not impact the proton concentration significantly, even at low concentrations of H_2. The simulations were then expanded to include doubly hydrogenated vacancies. These VH_2 defects have a slightly larger barrier for proton release (~0.6 eV), but are expected to be present in concentrations ten times larger than VH defects. When holes arrive at VH_2 sites, they can release a proton according to the following reaction:

$$h^+ + VH_2 \rightarrow VH + H^+ . \qquad (3.6)$$

This reaction significantly increases the proton concentration when low concentrations of H_2 are present, providing a mechanism for proton production in the absence of excess

molecular hydrogen. Note that the hydrogenated defects referred to in this section are dimer precursors. Puckered vacancy precursors are present at one tenth of the concentration of dimer vacancy precursors.

The formation of VH_2 defects requires H_2 to dissociate at neutral oxygen vacancies and form two Si-H bonds and the reaction barrier for this reaction is between ~2.4 eV and ~4 eV [11]. Fig. 3.5 shows the reaction energy for the lowest energy barrier case for the process. The high energy barrier makes the reaction unlikely to occur at room temperature. This reaction is possible at high temperatures, so the initial concentration of hydrogenated vacancies have to be formed during high temperature processing and annealing steps [11].

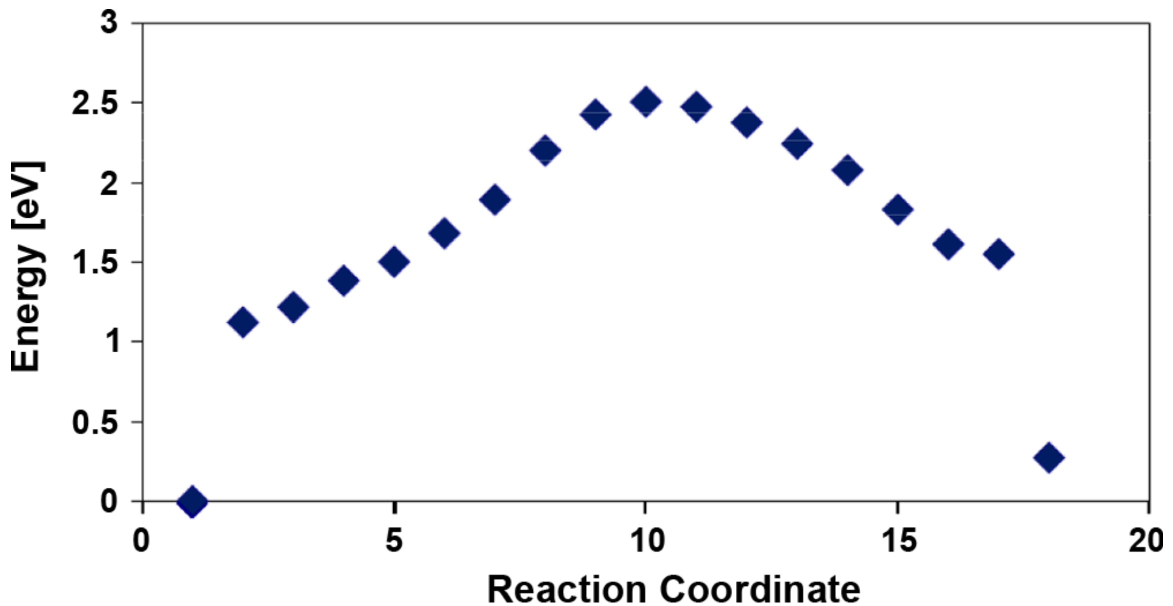

Fig. 3.5. Reaction energies for the dissociation of H_2 at a neutral oxygen vacancy to create a doubly hydrogenated vacancy [11].

In the presence of low concentrations of molecular hydrogen, proton generation is mainly due to the release of protons from doubly hydrogenated oxygen vacancies created during processing. When high concentrations of molecular hydrogen are present, proton generation is enhanced by the dissociation of H_2 at positively charged oxygen vacancies in the puckered configuration. Rowsey et al. [43] implement these mechanisms along with hole and electron capture and recombination at these defects and successfully simulate both interface-trap buildup that matches experimental data of hydrogen enhanced degradation and dose rate effects at varying concentrations of H_2. These results are shown in Figs. 3.6 and 3.7.

The mechanisms identified by this study explain how interface traps are formed at high and low concentrations of molecular hydrogen. The specific defects involved in these mechanisms are identified, providing a more physical understanding of the processes. The simulation results presented in Figs. 3.6 and 3.7 illustrate the robustness of these reactions in describing interface-trap formation under different conditions and explaining experimental results showing enhanced interface-trap buildup in the presence of hydrogen and changes in dose rate behavior.

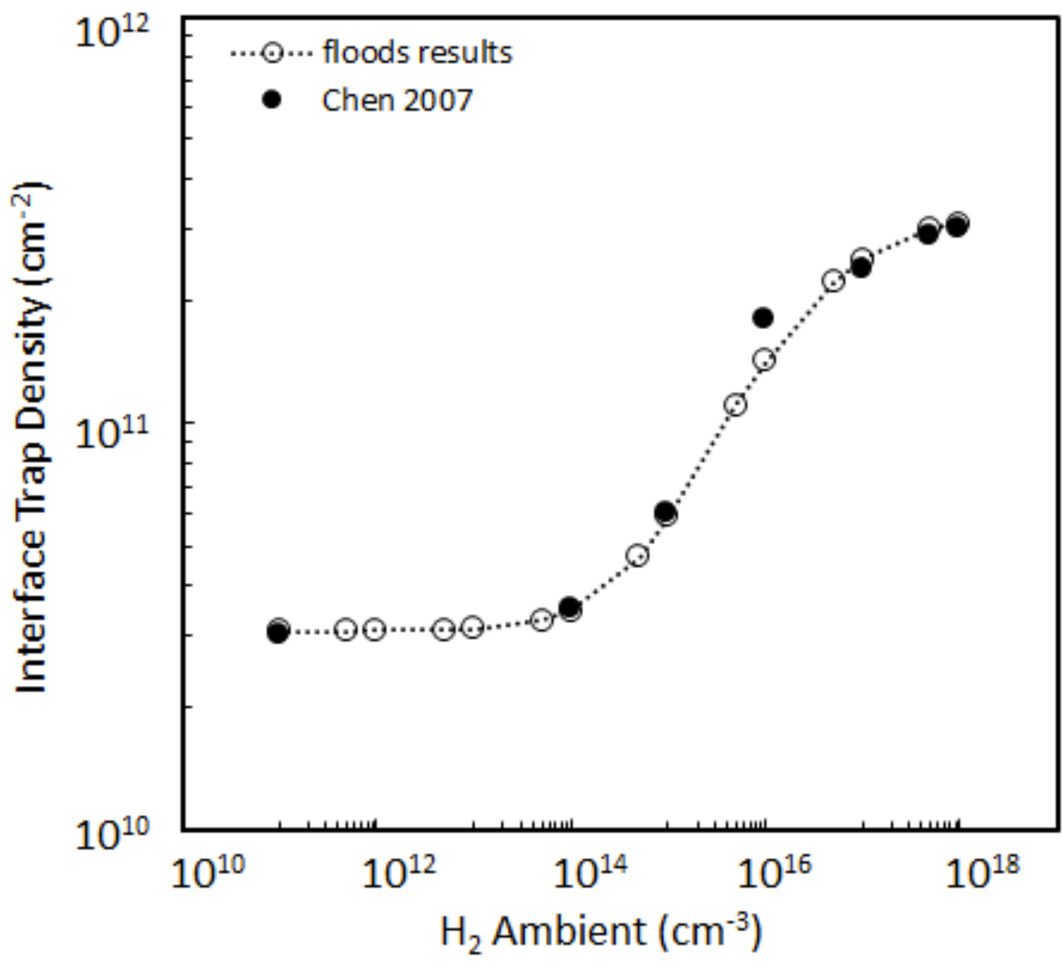

Fig. 3.6. Simulation results compared to experimental data from [4] showing interface-trap buildup as a function of molecular hydrogen concentration [43].

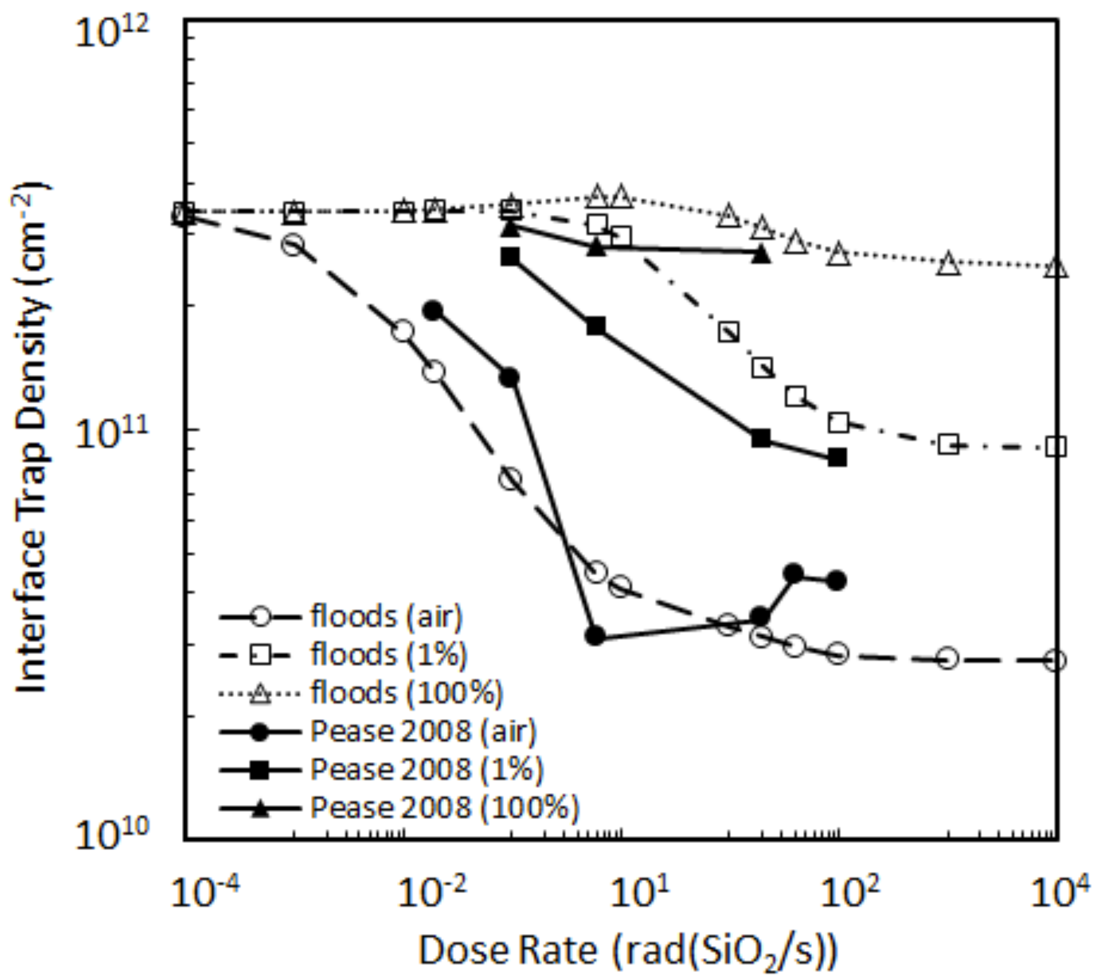

Fig. 3.7. Simulation results compared to experimental data from [19] showing interface-trap buildup as a function of dose rate for three different concentrations of molecular hydrogen concentration [43].

CHAPTER IV

PROTON LOSS AT ELEVATED TEMPERATURES - ANALYTICAL MODEL

Insights from the DFT calculations can be applied to studies investigating radiation response at elevated temperatures to help understand the enhanced interface-trap buildup and annealing that can occur under those conditions. In this chapter the effects of elevated temperature irradiation (ETI) are approached analytically. This analysis considers one of the proton loss mechanisms and compares the reaction rate coefficient of hydrogen dimerization at VH defects with proton release from VH_2 defects. The results indicate that reverse reactions become favorable at elevated temperatures that remove protons from the oxide and limit interface-trap formation. This forms the foundation for more in-depth numerical simulations of elevated temperature behavior.

Experimental Observations

ETI experiments show that the concentration of radiation-induced interface traps at a given dose rate depend on both the irradiation temperature and total dose [1]. In experiments by Witczak et al., shown in Fig. 4.1 [1], increasing irradiation temperature initially increases the excess base current of lateral *pnp* transistors, which is directly related to interface-trap buildup in these devices [62]. At even higher irradiation temperatures, however, the observed degradation can saturate or even decrease. The total dose dependence of the device response during these experiments is illustrated in Fig. 4.2 [1]. For a given total dose, the degradation increases with temperature until it reaches a

maximum, and then decreases with further increases in temperature. The transition from degradation to recovery occurs at lower temperatures for increasing total dose.

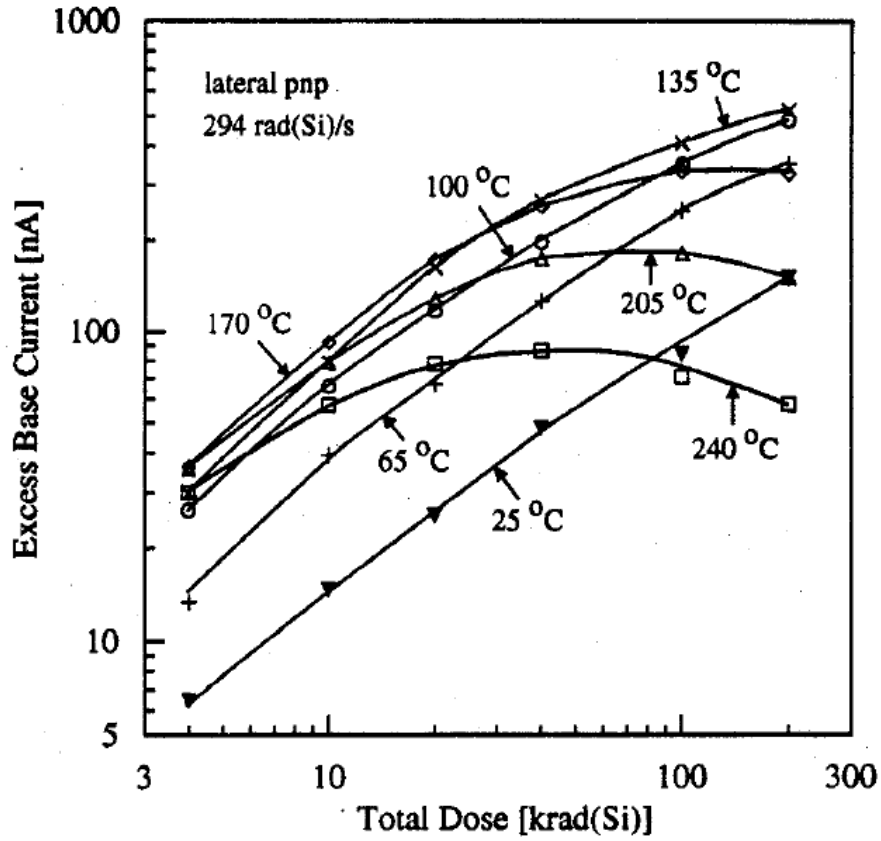

Fig. 4.1. Excess base current for a lateral PNP transistor as a function of total dose for seven different irradiation temperatures [1].

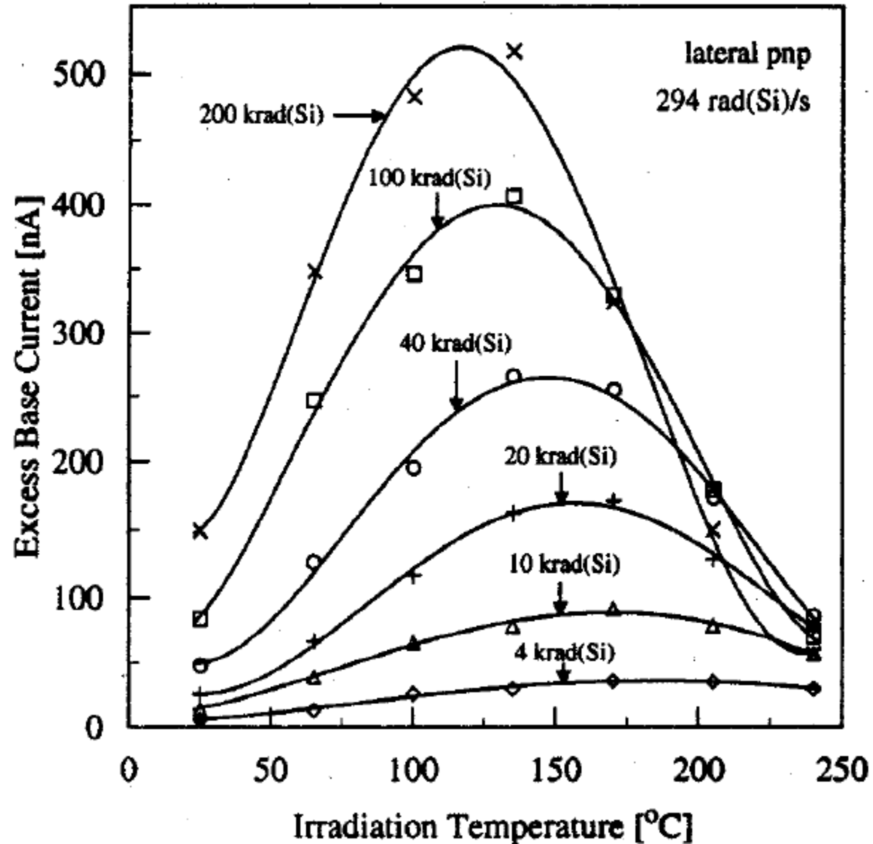

Fig. 4.2. Excess base current for a lateral PNP transistor as a function of irradiation temperature for six different total doses [1].

Proton Generation and Trapping

As irradiation temperature and total dose increase, Figs. 4.1 and 4.2 [1] show that the amount of degradation due to interface traps first increases, and then decreases. This is due to a competition between passivation and depassivation reactions at the interface. These reactions are limited by the relative supply of protons and molecular hydrogen, which can create and anneal interface traps, respectively. Protons can be generated from H_2 cracking at $V_{o\gamma}^+$ defects according to reaction (3.4) and from direct proton release via holes from VH_2 defects according to reaction (3.6). Protons can also be trapped at defects, as mentioned when discussing the possibility of H_2 cracking at $V_{o\delta}^+$ defects,

reaction (3.3). These results indicate that it is energetically favorable for a proton to arrive at a hydrogenated vacancy, bond with the other hydrogen atom, and diffuse away as molecular hydrogen, leaving behind a positively charged oxygen vacancy [11]. This analysis considers the capture of protons at VH defects:

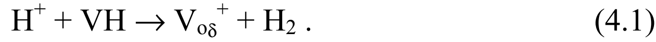

$$H^+ + VH \rightarrow V_{o\delta}^{\ +} + H_2 \ . \qquad (4.1)$$

This process is referred to as hydrogen dimerization, i.e., when two atomic hydrogens combine to form molecular hydrogen. In this case one atom is the free moving proton and the other atom is part of a Si-H bond. If this reaction works efficiently, it has a large effect on the interface-trap density. Protons are neutralized in the reaction, something that is very unlikely to occur directly due to a small electron capture cross section [17], and the remaining positive charge is at a shallow trap, which has a much larger cross section for electron capture [17].

Reaction Rates

The competition between proton generation and recombination determines how many protons can reach the interface and create interface traps. The effects of proton release at VH_2 defects (3.6) and hydrogen dimerization at VH defects (4.1) on the proton concentration can be compared by examining the proton continuity equation:

$$\frac{\partial[\mathrm{H}^+]}{\partial t} = k_1[\mathrm{h}^+][\mathrm{VH}_2] - k_2[\mathrm{H}^+][\mathrm{VH}] - \nabla \cdot f_{H^+}. (4.2)$$

Here k_1 and k_2 are reaction rate coefficients and f_{H+} is the proton flux (number per unit area per unit time). The first term is the reaction rate for proton release, which depends on k_1, the concentration of holes, and the concentration of VH_2 defects. The second term is the reaction rate for dimerization, which depends on k_2 and the concentrations of protons

and VH defects. Increases in the reaction rate for proton release increase the proton concentration in the oxide. Increases in the reaction rate for dimerization decrease the proton concentration and increase the H_2 concentration. Both the reaction rate coefficients and the reactant concentrations change with temperature.

The initial increase in interface-trap density with temperature in the bipolar base oxides reported in Figs. 4.1 and 4.2 occurs primarily because of the increase in proton concentration as the reaction rate for proton release at VH_2 defects via holes (3.6) increases. As the temperature increases, the reaction rate coefficient for proton release, k_1, increases, generating protons more rapidly. The equation for an arbitrary reaction rate coefficient of this type is given by:

$$k_n = L_c \times D \times \exp(-E_b/k_B T). \qquad (4.3)$$

where L_c is the capture length of the defect, D is the diffusivity of the diffusing species, E_b is the reaction barrier, k_B is the Boltzmann constant, and T is the temperature. For proton release, the holes are the diffusing species, and for dimerization protons are the diffusing species. The DFT calculations already account for the diffusion barrier, so that must be subtracted in order to obtain the energy barrier. In addition to the temperature dependence of the energy barrier term, the diffusivity also depends exponentially on temperature:

$$D = D_0 \times \exp(-E_d/k_B T). \qquad (4.4)$$

Here D_0 is a constant and E_d is the diffusion energy. As temperature increases, the values of the energy barrier exponential and the diffusivity increase, accelerating the reaction. Increases in temperature increase the effective charge yield by reducing space charge effects, which cause enhanced electron-hole recombination in SiO_2 [27], increasing the

reaction rate as well. Proton diffusivity also increases with temperature, hastening transport to the interface. The combination of a higher rate of proton release and higher mobility for protons results in increased interface-trap creation with increasing temperature.

As temperature increases further, interface-trap buildup slows and even decreases as the total dose (and thus the irradiation time) increases. As stated before, interface-trap density is affected by the relative supply of protons and molecular hydrogen near the interface, so the first notable observation is that the maximum reaction rate for proton dimerization is near the interface. This is because the reaction rate in (4.3) depends on the concentration of protons and VH defects, both of which are greatest near the interface. Protons build up there as they are released in the bulk oxide, and VH defects increase there as well. This is because VH defects naturally comprise a percentage of the oxygen vacancy defects after typical device processing [11], and the concentration increases near the interface along with the concentration of oxygen vacancies [63]. This is illustrated in Fig. 4.3.

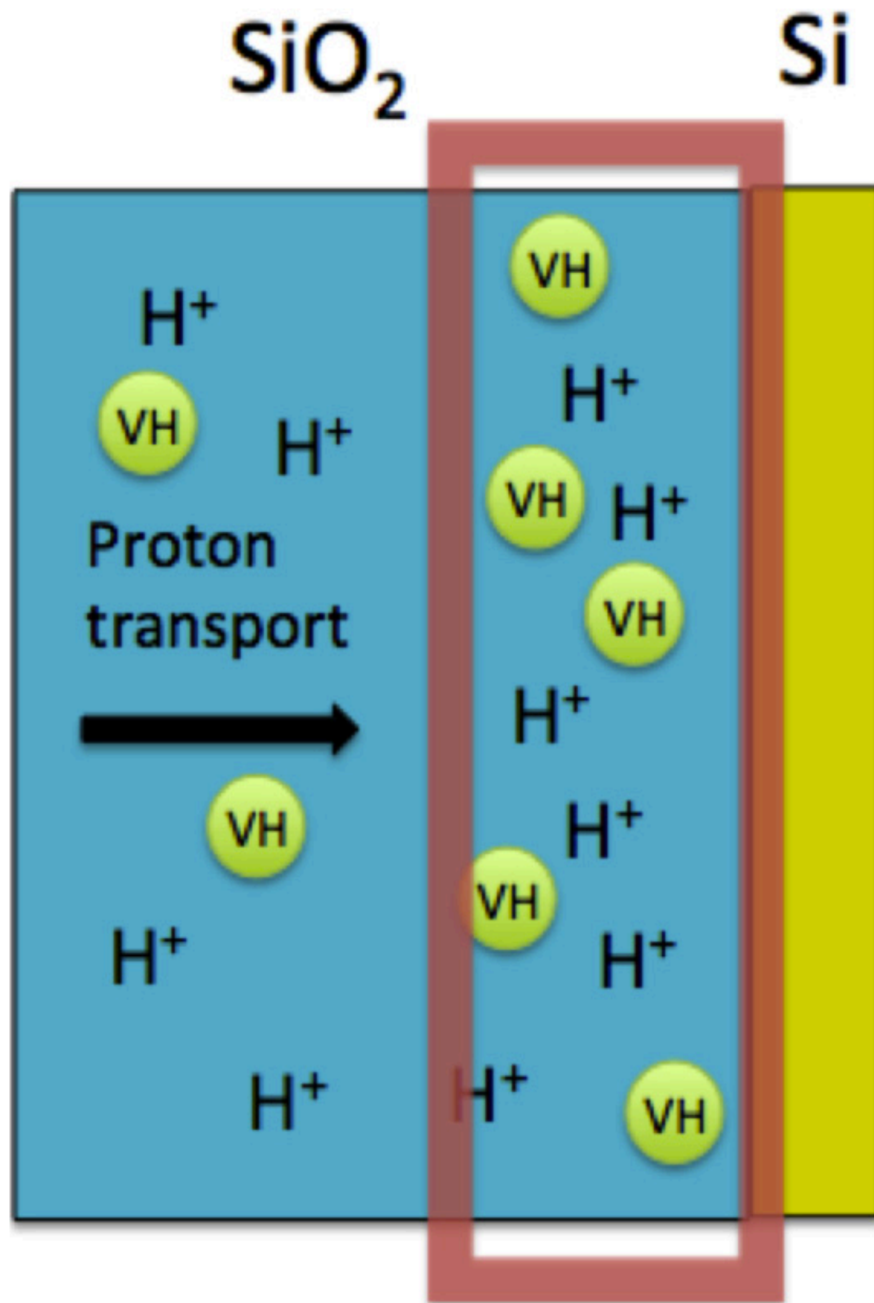

Fig. 4.3. View of the oxide showing the relative concentrations of protons and VH defects in the oxide.

Note that $V_{o\delta}$ defects are also potential trapping sites for protons and the same logic about near interfacial concentration increase applies to those defects as well.

Competing Reactions at Elevated Temperatures

Increases in the rate of dimerization favor annealing reactions by decreasing the proton concentration and increasing the H_2 concentration. According to (4.3), the reaction rate coefficient increases with temperature because of the energy barrier exponential and the diffusivity. The energy barrier provided by the DFT calculations includes the diffusion barrier for the diffusing species, which must be subtracted because the diffusion energy is already accounted for in the diffusivity term, as seen in (4.4). The calculated barrier for dimerization is ~0.8 eV [11], and the diffusion energy of protons is also 0.8 eV [64]-[66], so hydrogen dimerization occurs at VH defects without a barrier. This means that the temperature dependence of the reaction rate coefficient is completely due to changes in the diffusivity of protons. The barrier for proton release is ~0.5 eV [43], however, there have been many numbers reported for the activation energy for hole transport and the actual value varies based on factors like the electric field and oxide quality [67]. For the purposes of this analysis, a value of 0.4 eV is used, taken from [68]. The difference is only 0.1 eV, so the majority of the temperature dependence on the reaction rate coefficient for proton release is due to changes in the diffusivity of holes.

Direct dimerization of two neutral atomic hydrogen atoms (forming H_2) has been proposed as a mechanism to limit interface-trap buildup at high dose rates [13]. However, there is little evidence that neutral atomic hydrogen exists in significant quantities in the oxide at or above room temperature, and other mechanisms involving competition

between proton release and electron–hole recombination have also been invoked to explain ELDRS [16], [17]. The calculations of [11] show that a dimerization reaction involving protons can occur at a VH defect. However, at room temperature this reaction is not very efficient and few protons react at VH defects. The efficiency of hydrogen dimerization is determined by the second term in (4.2), the reaction rate. The reaction rate increases with temperature as both the reaction rate coefficient and the proton concentration increase. The temperature dependent terms of the reaction rate coefficient are the energy barrier exponential and the diffusivity, which can be seen in (4.3) and (4.4). The changes in these terms with temperature are different for proton release and hydrogen dimerization and contribute to the change from enhanced degradation to enhanced annealing seen in Figs. 4.1 and 4.2.

As noted previously, the diffusivity of protons and holes show the most variability with temperature. For proton release, the diffusing species are holes, and for hydrogen dimerization the diffusing species are protons. The diffusivity has an exponential dependence on temperature, as seen in (4.4). The activation energy for proton transport is ~0.8 eV [62], [64], [66], [68]. For holes, there have been many numbers reported and the actual value varies based on factors like electric field and oxide quality [67]. We use a value of 0.4 eV for this analysis, taken from [69]. Rashkeev et al. [12] use drift-diffusion modeling for hole transport and a range of effective mobility values, the average value being 10^{-7} cm^2/Vs. Applying the Einstein relation, $D = \mu k_B T$, the room temperature diffusivity of holes is ~2.5×10^{-9} cm^2/s. Holes transport much faster than protons [37], so in this thesis a representative value for room temperature proton diffusivity of ~2.5×10^{-12} cm^2/s is used, three orders of magnitude lower than that of the holes. Similar values

have been used previously in simulations of the oxides overlying the base region of bipolar transistors [42]. The trends in the temperature response are not affected strongly by the particular choices of the diffusivities. From these values and the activation energies reported in the literature, a diffusivity equation in the form of (4.4) is written for each species and the results are plotted in Fig. 4.4. The diffusivity of protons, which affects the reaction rate coefficient of hydrogen dimerization, increases faster with increasing temperature than the diffusivity of holes, which affects the reaction rate coefficient of proton release.

The resulting reaction rate coefficients for proton release and hydrogen dimerization are plotted in Fig. 4.5. The value used for capture length, L_c, from (4.3), is 3 Å, the average distance between oxygen atoms. The reaction rate coefficient for hydrogen dimerization has a stronger temperature dependence than the reaction rate coefficient for proton release. For these values, at room temperature the reaction rate coefficient comparison favors proton release by an order of magnitude, but at elevated temperatures the comparison favors dimerization by an order of magnitude for a change of about 200K.

Ultimately, the proton concentration near the interface is determined by the reaction rates of proton release and hydrogen dimerization, the first two terms on the right-hand side of (4.2). At elevated temperatures, the reaction rate coefficient for dimerization is an order of magnitude higher than proton release. Other factors like relative concentrations of molecular hydrogen versus protons and hydrogenated oxygen vacancies versus oxygen vacancies help determine which reaction dominates. Increases in the rate of proton release throughout the oxide results in a large buildup of protons as

they transport to the interface. This large concentration of protons near the interface drives the dimerization reaction rate higher as well, causing a net loss of protons near the interface. The rate of interface-trap creation depends on the availability of protons near the interface, and the reduction in proton concentration lowers this rate. Hence, the buildup of interface traps begins to saturate with increasing temperature, as seen in Fig. 4.2.

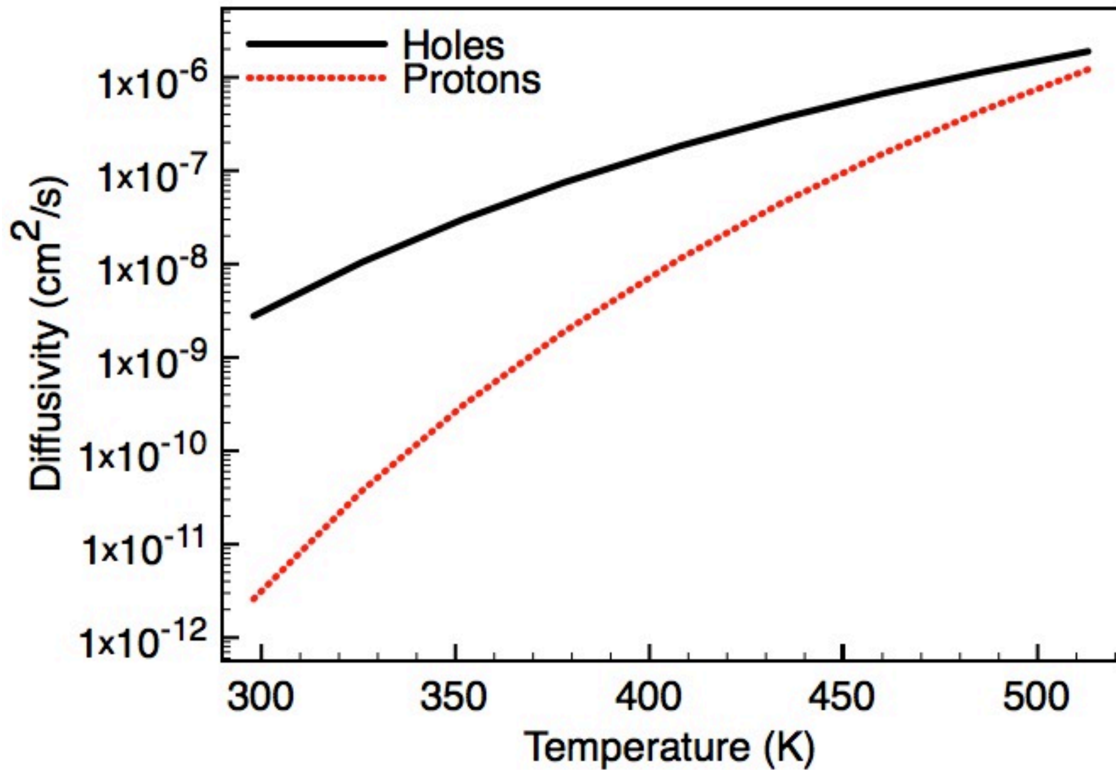

Fig. 4.4. Value of the diffusivity for protons and holes as a function of temperature.

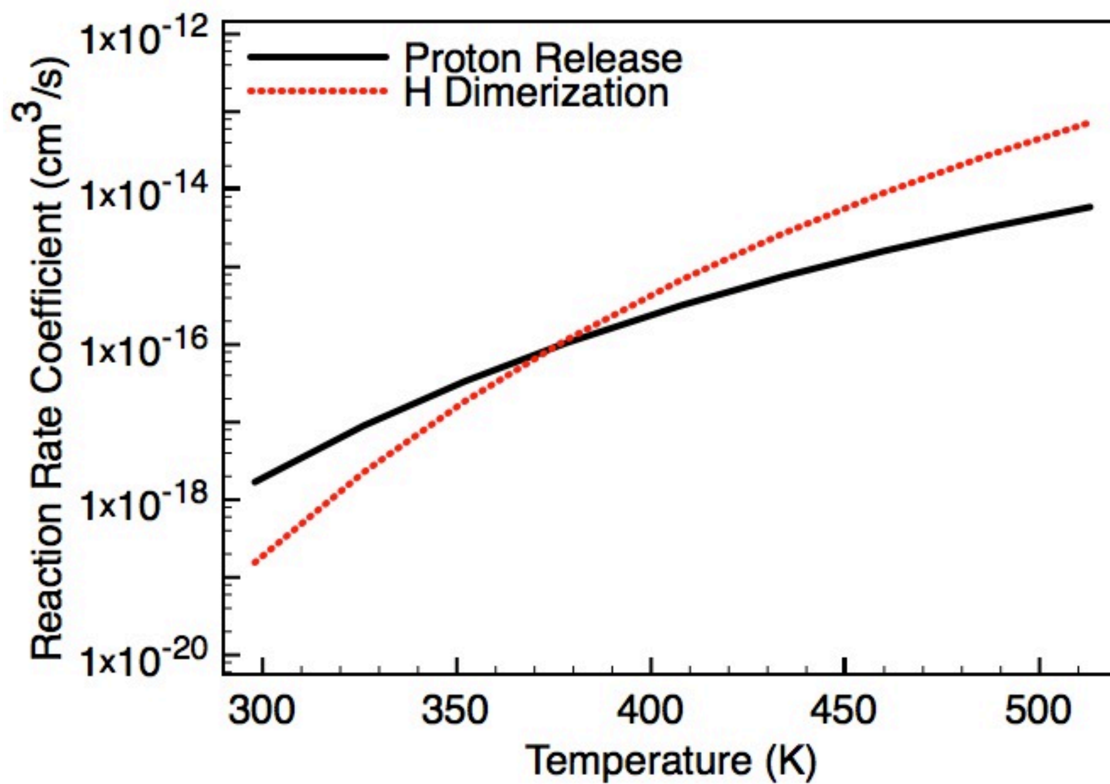

Fig. 4.5. Value of the reaction rate coefficient for proton release and hydrogen dimerization as a function of temperature.

CHAPTER V

INTERFACE TRAP BUILDUP AND ANNEALING AT ELEVATED TEMPERATURES - NUMERICAL MODEL

Interface-trap buildup and annealing as a function of temperature, dose rate, and H_2 concentration are simulated numerically using a physics-based model. The roles of a number of common oxide defects in radiation-induced interface-trap buildup are evaluated under various conditions. Previously, Rashkeev et al. [37] demonstrated that interface-trap buildup is affected by proton mobility and that there is a temperature-dependent competition between interface-trap formation and annealing reactions at the interface. Higher temperatures favor passivation reactions, contributing to the reduction in interface-trap density seen with increasing annealing temperatures in MOSFETS. The roles of defects other than interface traps have not been investigated in detail. References [13] and [16] discuss how defects in the oxide affect radiation response, focusing on dose rate sensitivity using a variety of bimolecular reactions at generic defects to fit the data. Reference [43] reports a physics-based approach to simulate the effects of dose rate and increased H_2 concentration.

The model presented here simulates interface-trap buildup at varying temperature, H_2 concentration, and dose rate for a 1-D slice of silicon dioxide and silicon. The simulations use defects identified by first principles calculations [11] as likely candidates to be in typical oxides and implements reactions with calculated energy barriers to create a model that describes interface-trap buildup under a variety of conditions. The results are

compared to experimental data and defects that control interface-trap buildup under different conditions are identified. The implications of different limiting mechanisms at elevated temperatures and low dose rate for accelerated testing at elevated temperatures are discussed.

Model Details

The buildup and annealing of interface traps is numerically simulated using the FLorida Object Oriented Device Simulator (FLOODS) [70] over a range of temperatures and H_2 concentrations. FLOODS is a TCAD device simulator that models the transport and reactions of species in the oxide. It solves coupled differential equations at discrete points on a grid using the finite-element and finite volume techniques [71], [72] describing the electric field, transport, and generation and recombination terms. Rowsey et al. [43] use the same tool to simulate dose rate effects in bipolar oxides. The condition under study is for low electric fields, so a value of ~10 kV/cm is used. The simulations incorporate reactions at both dimer and puckered configurations of oxygen vacancies, V_o, hydrogenated oxygen vacancies, VH, and doubly hydrogenated oxygen vacancies, VH_2. The energy barriers for these reactions are calculated using density functional theory and implemented in the model. The calculated energy barriers are fixed within a margin of error of 0.1 eV. Reaction rates are computed in the simulations as a reaction rate coefficient times the concentration of the reactants. The formula for the reaction rate coefficient for reactions with a mobile and immobile species is:

$$L_c \times D \times e^{(-Ea/kT)} . \qquad (5.1)$$

L_c is the capture length of the defect, D is the diffusivity of the mobile species, E_a is the

reaction barrier, k is the Boltzmann constant, and T is the temperature. The value used for capture length for reactions with uncharged species is 3 Å, and the value used for reactions with charged species is 3 nm. The diffusivities are calculated in the same manner described in chapter IV. The forward and reverse energy barrier is calculated for each reaction. Note that some of the reactions listed previously were simplified reactions with an immobile and mobile species on each side of the reaction. For example, reaction (3.6) describes a hole arriving and releasing a proton from a VH_2 defect and reaction (4.1) describes a proton being trapped at a VH defect to release a hydrogen molecule. This formulation takes into account the intermediate stage of every reaction for a more physical description of the processes. For example, the process of proton release via a hole at a VH_2 defect (3.6) is simulated as a hole being trapped at a VH_2 defect, producing a positively charged defect, VH_2^+. Then, the VH_2^+ may release a proton as in reaction (3.6). Once the hole is trapped at the VH_2 defect, releasing a proton is not the only possible reaction. An H_2 molecule may be released instead, leaving behind a positively charged oxygen vacancy or the hole may simply detrap. The reaction rate for each of these reactions determines which process occurs. For reactions with an immobile and mobile species, equation (5.1), consisting of the product of the capture length, diffusivity, and energy barrier exponential, determines the reaction rate coefficient. For an immobile species, the reaction rate coefficient is calculated as an attempt to escape frequency multiplied by the energy barrier exponential. The attempt to escape frequency used for holes is 5×10^{13} s^{-1}, within the range of values typically reported in the literature [73]. The attempt to escape frequency used for hydrogen is 10^{13} s^{-1}, based on the vibrational frequency of hydrogen [74]. All reactions are listed below with their forward and reverse

energy barriers listed next to them in the form (E_f, E_r) and then the equation number farthest to the right. E_f is forward energy barrier and E_r is reverse energy barrier.

$h^+ + V_{o\gamma} \Leftrightarrow V_{o\gamma}^+$. (0.0, 4.5) (5.2)

$e^- + V_{o\gamma}^+ \Leftrightarrow V_{o\gamma}$. (0.4, 9.0) (5.3)

$h^+ + V_{o\delta} \Leftrightarrow V_{o\delta}^+$. (0.0, 0.6) (5.4)

$e^- + V_{o\delta}^+ \Leftrightarrow V_{o\delta}$. (0.4, 9.0) (5.5)

$h^+ + V_\gamma H \Leftrightarrow V_\gamma H^+$. (0.0, 4.5) (5.6)

$V_\gamma H^+ \Leftrightarrow V_{o\gamma} + H^+$. (2.0, 1.8) (5.7)

$e^- + V_\gamma H^+ \Leftrightarrow V_\gamma H$. (0.4, 7.5) (5.8)

$h^+ + V_\delta H \Leftrightarrow V_\delta H^+$. (0.0, 0.6) (5.9)

$V_\delta H^+ \Leftrightarrow V_{o\delta} + H^+$. (0.4, 0.6) (5.10)

$e^- + V_\delta H^+ \Leftrightarrow V_\delta H$. (0.4, 3.0) (5.11)

$h^+ + V_\gamma H_2 \Leftrightarrow V_\gamma H_2^+$. (0.0, 0.6) (5.12)

$V_\gamma H_2^+ \Leftrightarrow V_\gamma H + H^+$. (0.4, 0.8) (5.13)

$V_\gamma H_2^+ \Leftrightarrow V_{o\gamma}^+ + H_2$. (0.3, 0.6) (5.14)

$e^- + V_\gamma H_2^+ \Leftrightarrow V_\gamma H_2$. (0.4, 9.0) (5.15)

$h^+ + V_\delta H_2 \Leftrightarrow V_\delta H_2^+$. (0.0, 0.6) (5.16)

$$V_\delta H_2^+ \Leftrightarrow V_\delta H + H^+ . \qquad (0.6, 0.7) \qquad (5.17)$$

$$V_\delta H_2^+ \Leftrightarrow V_{o\delta}^+ + H_2 . \qquad (0.5, 1.2) \qquad (5.18)$$

$$e^- + V_\delta H_2^+ \Leftrightarrow V_\delta H_2 . \qquad (0.4, 9.0) \qquad (5.19)$$

Varying H_2 Concentration

The simulation results are plotted in Fig. 5.1, which shows interface-trap concentration vs. temperature for different H_2 concentrations in the oxide. Simulations are performed over a wide range of H_2 concentrations, 5×10^{13} cm^{-3} to 5×10^{21} cm^{-3}, since levels may vary widely from part to part and between different processes. The lowest value, 5×10^{13} cm^{-3}, is an unphysically low hydrogen concentration, and is chosen as a lower bound for parts that have been manufactured to limit hydrogen in the oxide. The highest value, 5×10^{21} cm^{-3}, represents a part with excess H_2 introduced, e.g., as a result of outgassing from the packaging. The oxide simulated is 0.57 μm (from [1]), with a 4 nm section near the interface where defect values increase to a higher peak density. A peak value of 10^{20} cm^{-3} near the interface for $V_{o\delta}$ defects is used, with appropriately scaled concentrations for the rest of the defects, based on the ratios described previously. The thickness of the oxide impacts the magnitude of the interface-trap buildup, but not the shape of the curves. Similarly, fluctuations in the defect concentrations shift the magnitude of the interface-trap buildup, sometimes only at specific temperatures, but the general shape of the temperature profile for interface-trap buildup remains constant. Thus, any conclusions about the system are broadly applicable.

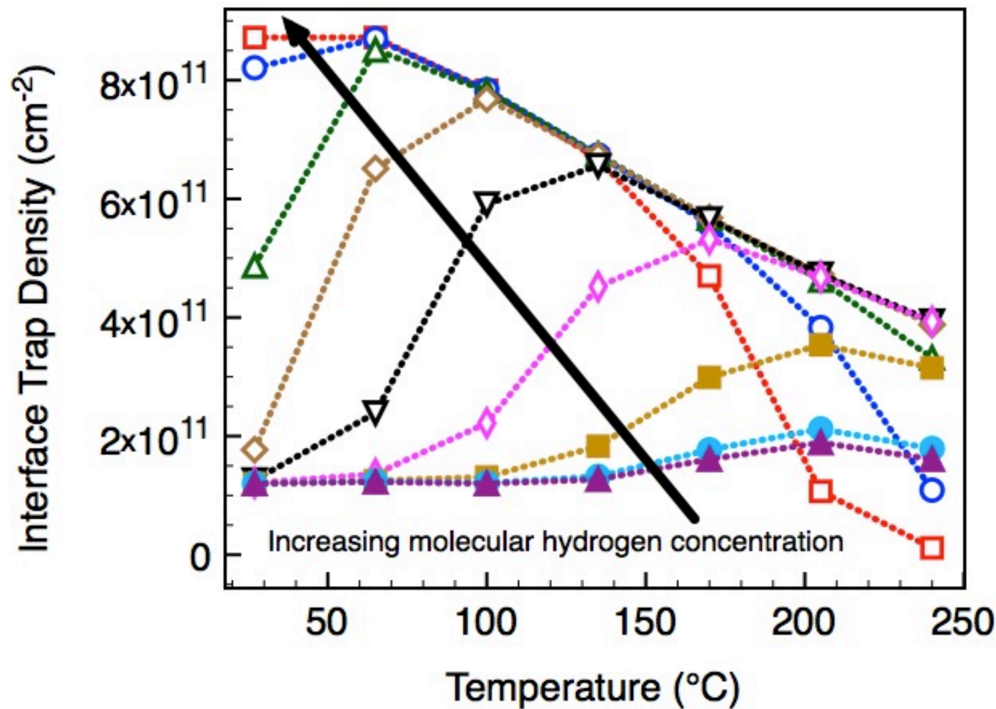

Fig. 5.1. Simulated interface-trap buildup versus temperature for varying concentrations of H_2 in the oxide. The H_2 levels assumed in the calculations range from 5×10^{13} cm^{-3} to 5×10^{21} cm^{-3}. The total dose is 40 krad(SiO_2).

Comparison to Experimental Data

Simulation results are compared to data from [1]. Using the same conditions as [1], the dose rate is 294 rad(SiO_2)/s and the total dose is 40 krad(SiO_2). The simulations in the mid-range of H_2 concentration, 5×10^{17} cm^{-3}, produce results similar to the data from [1]. Total doses of 20 krad(SiO_2) and 10 krad(SiO_2) are also simulated for comparison to the experimental data in Fig. 4.2. Fig. 5.2 plots the simulated interface-trap buildup versus temperature for the three total doses at an H_2 concentration of 5×10^{17} cm^{-3}. The excess base currents measured from [1] for the same three total doses are plotted on the second y-axis. Measurements from [1] for elevated temperatures are taken

after cooling the device down to room temperature.

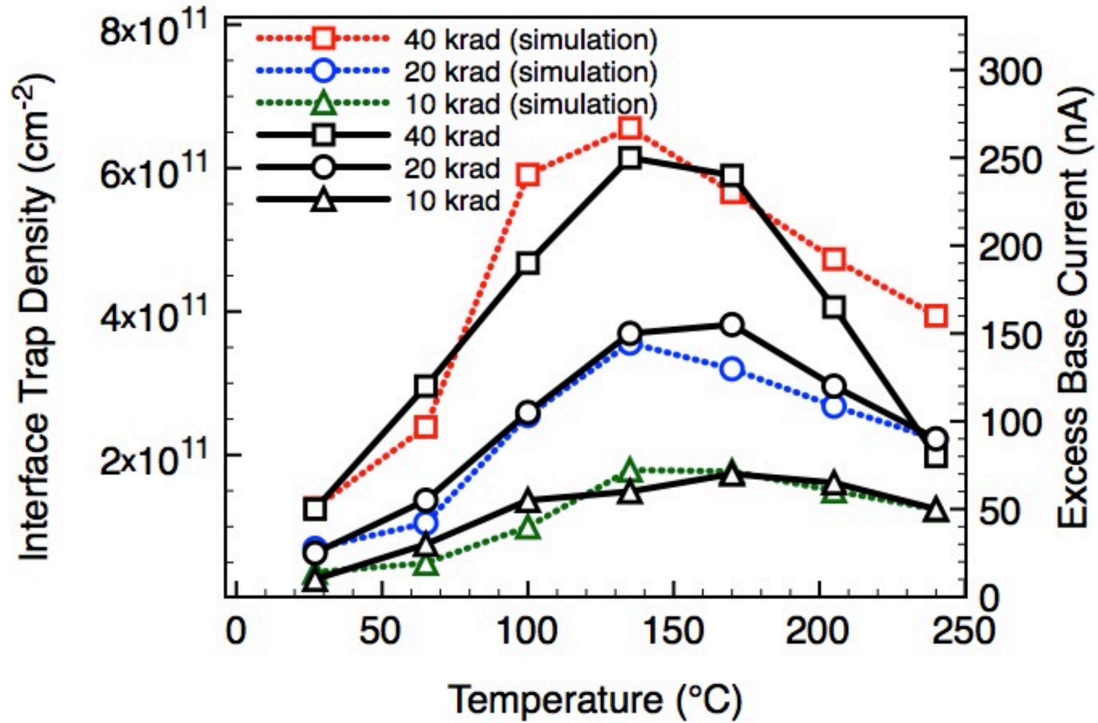

Fig. 5.2. Simulated interface-trap buildup versus temperature for total doses of 10, 20, and 40 krad(SiO_2) at 294 rad/s, with excess base current plotted on the second y-axis for measurements reported in [1] with the same dose rate and total doses. The H_2 concentration in the simulation is 5×10^{17} cm^{-3}.

Contributions of Proton Loss Reactions

Proton-defect reactions near the interface contribute to decreased interface-trap buildup by lowering the proton concentration near the interface. Simulations without these reactions show the temperature range over which they are limiting mechanisms. To turn off a certain reaction, the barrier for that reaction is raised by 1 eV, ensuring that the contribution of the reaction is negligible on the timescale of the simulations. Fig. 5.3 plots the interface-trap buildup for the simulation with normal reaction barriers, with the

capture of protons at $V_\delta H$ defects, the reverse reaction of (5.17), turned off, and with proton capture at $V_{o\delta}$ defects, the reverse reaction of (5.10), turned off. Note that no significant changes occur when increasing the energy barrier for proton capture at $V_\gamma H$ defects due to the lower concentration of those defects. Also, the barrier for capture of protons at $V_{o\gamma}$ defects is too high to have an impact on these simulations. The results show that at higher temperatures, both of these reactions limit interface-trap buildup. Above 100°C, when there is no proton capture at $V_{o\delta}$ defects, degradation increases by 2× or more over the baseline case and little decrease is seen after saturation.

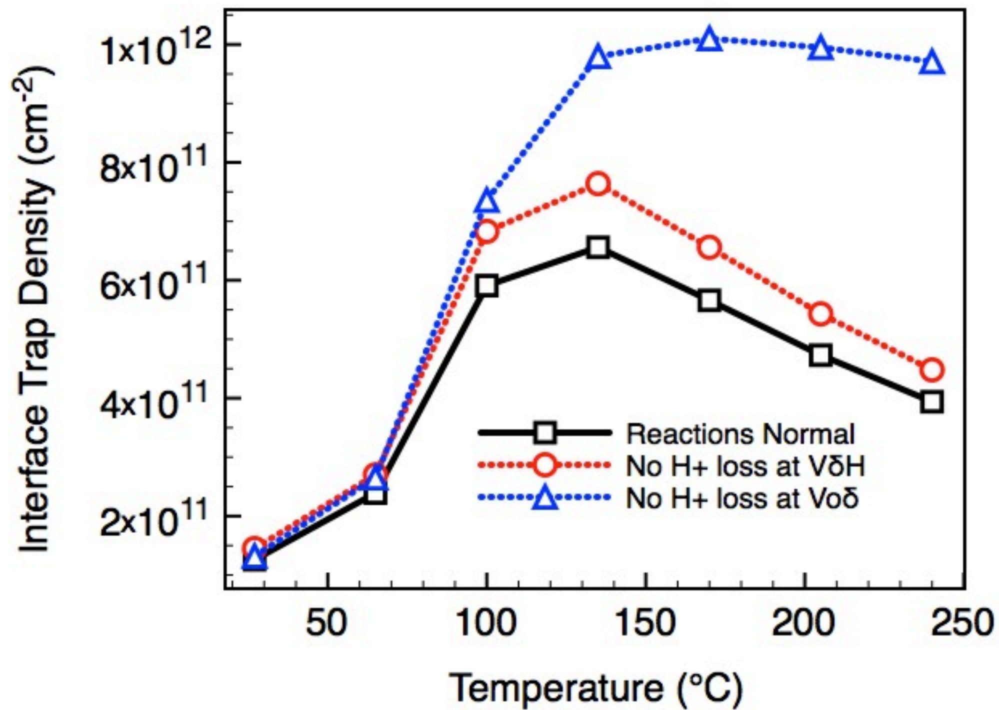

Fig. 5.3. Simulated interface-trap buildup versus temperature with proton capture at $V_{o\delta}$ defects suppressed (dashed blue), defect-mediated dimerization at $V_\delta H$ defects suppressed (dashed red line), and with normal reactions (solid black line) with the H_2 concentration at 5×10^{17} cm^{-3}.

Variations in Defect Concentration

Simulations altering the concentration of defects individually are performed in order to evaluate the sensitivity of interface-trap buildup to individual defects. Changes in the concentrations of $V_{o\delta}$ and $V_{o\gamma}$ defects have the most impact on interface-trap buildup. The results for varying the $V_{o\delta}$ and $V_{o\gamma}$ concentrations are plotted in Fig. 5.4. At elevated temperatures, $V_{o\delta}$ defects remove a significant amount of protons from the oxide via the reverse reaction of (5.10), limiting interface-trap buildup, resulting in an inverse relationship between $V_{o\delta}$ defects and proton supply. Consequently, increasing the concentration of $V_{o\delta}$ defects decreases the proton supply and decreasing that concentration increases the proton supply. At this concentration of H_2, protons are primarily produced at $V_{o\gamma}$ via reaction (5.13). Thus, there is a direct relationship between $V_{o\gamma}$ defects and proton supply, where increasing the concentration of $V_{o\gamma}$ defects increases the proton supply and decreasing that concentration decreases the proton supply.

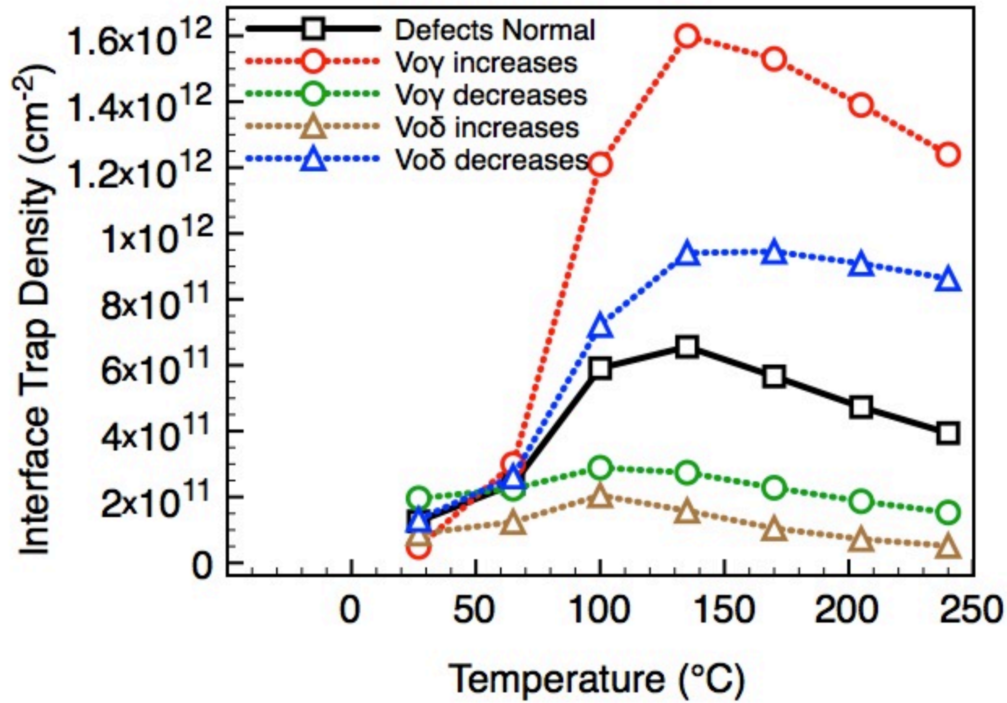

Fig. 5.4. Simulated interface-trap buildup versus temperature with an order of magnitude increase or decrease in $V_{o\delta}$ defects and $V_{o\gamma}$ defects with the H_2 concentration at 5×10^{17} cm^{-3}.

For low H_2 levels, interface-trap buildup is lower than that with high H_2 concentrations (Fig 5.1). The low H_2 concentration suppresses proton generation by reaction (5.13) because the formation of $V_\gamma H_2^+$ via the reverse of reaction (5.14) is reduced. As a result, $V_{o\gamma}$ defects have little effect and different mechanisms determine interface-trap buildup. Variations in interface-trap density with changing defect concentrations for this H_2 concentration are plotted in Fig. 5.5. The primary source of protons is reaction (5.17), direct release from hydrogenated vacancies. This can be seen by the increases in interface-trap density with increasing $V_\delta H_2$ concentration. Varying the $V_{o\delta}$ concentration still produces an effect; however, decreasing the $V_{o\delta}$ defects has a less

significant impact on interface-trap buildup until the temperature is close to 200°C, compared to around 100°C at an H_2 concentration of 5×10^{17} cm^{-3}, due to the reduced proton production at these H_2 levels.

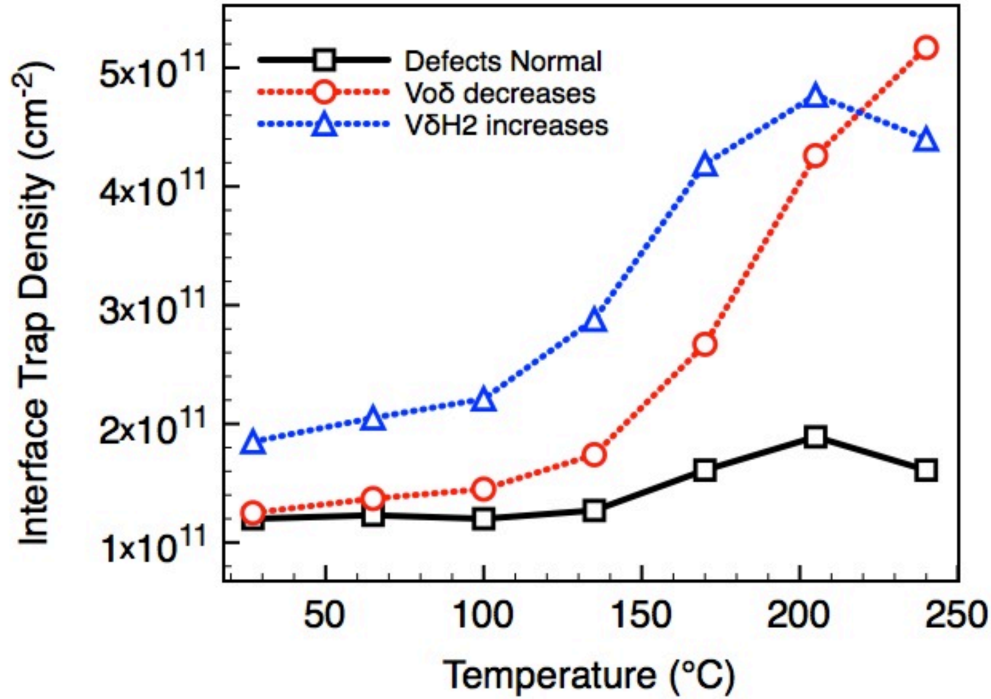

Fig. 5.5. Simulated interface-trap buildup versus temperature for an order of magnitude increase in $V_\delta H_2$ defects and an order of magnitude decrease in $V_{o\delta}$ defects with the H_2 concentration at 5×10^{13} cm^{-3}.

Varying H_2 Concentration and Temperature

For high H_2 levels, interface-trap buildup increases significantly at lower temperatures due to increased proton production via reaction (5.13), but falls off faster at higher temperatures, as seen in Fig. 5.1. At higher temperatures, passivation of interface traps dominates with such a large supply of H_2. The mechanisms of proton generation

and loss are the same as those at medium levels of H_2, so $V_{o\delta}$ and $V_{o\gamma}$ defects again have the largest effect on interface-trap buildup, similar to the results shown in Fig. 5.4. There is a direct relationship between $V_{o\gamma}$ defects and proton supply and an inverse relationship between $V_{o\delta}$ defects and proton supply.

Fig. 5.1 shows that interface-trap buildup can vary significantly over the range of 25°C to 240°C depending on the concentration of H_2 in the oxide. This is due to a number of competing reactions. Increasing the H_2 concentration increases the protons produced through reaction (5.13), H_2 dissociation, favoring increased interface-trap buildup. As the proton concentration increases, protons are captured near the interface by $V_\delta H$ and $V_{o\delta}$ defects via the reverse reactions of (5.10) and (5.17), suppressing interface-trap buildup. Additionally, higher H_2 concentrations favor passivation of interface traps. However, the barrier for passivation is very high, 1.3 eV [75], and only becomes a significant factor on the timescale of the simulations at elevated temperatures and high H_2 concentrations. Proton-capture processes at $V_{o\delta}$ and $V_\delta H$ defects are reverse reactions, with barriers of 0.6 eV and 0.7 eV, respectively. In reaction (5.13), proton release from a $V_\gamma H_2$ complex only has a 0.4 eV barrier. Note that while the capture of a hydrogen molecule to form this defect is also a reverse reaction, the significant quantity of H_2 present drives that reaction and is not the limiting process. As a result of the lower barrier for proton release, interface-trap buildup is enhanced at lower temperatures. However, as temperature increases and proton concentrations increase, proton capture at defects becomes more likely. Therefore, at mid-levels of H_2 concentration, increasing temperature initially produces a sharp increase in interface-trap buildup as proton production from $V_\gamma H_2^+$ defects, reaction (5.13), and $V_\delta H_2^+$ defects, reaction (5.17), is

enhanced. As temperature increases and proton levels rise, the proton concentration near the interface is modulated by proton capture at $V_\delta H$ defects, reaction (5.17), and $V_{o\delta}$ defects, reaction (5.10). So, as temperature increases, proton production increases, but proton capture at the interface prevents this increase from being fully realized.

As H_2 levels increase even further, more protons are created through dissociation at lower temperatures, but the large H_2 supply drives passivation to become a competing reaction on the timescale of the irradiation, resulting in the sharp decline in interface-trap buildup with temperature. With increased proton generation, proton losses are also significant at low temperatures, as seen in Fig. 5.6, where interface-trap buildup is plotted versus temperature at an H_2 concentration of 5×10^{21} cm^{-3} with proton loss reactions turned off. As interface-trap buildup is enhanced through increased proton release due to increased H_2 or higher temperatures, other reactions oppose this increase.

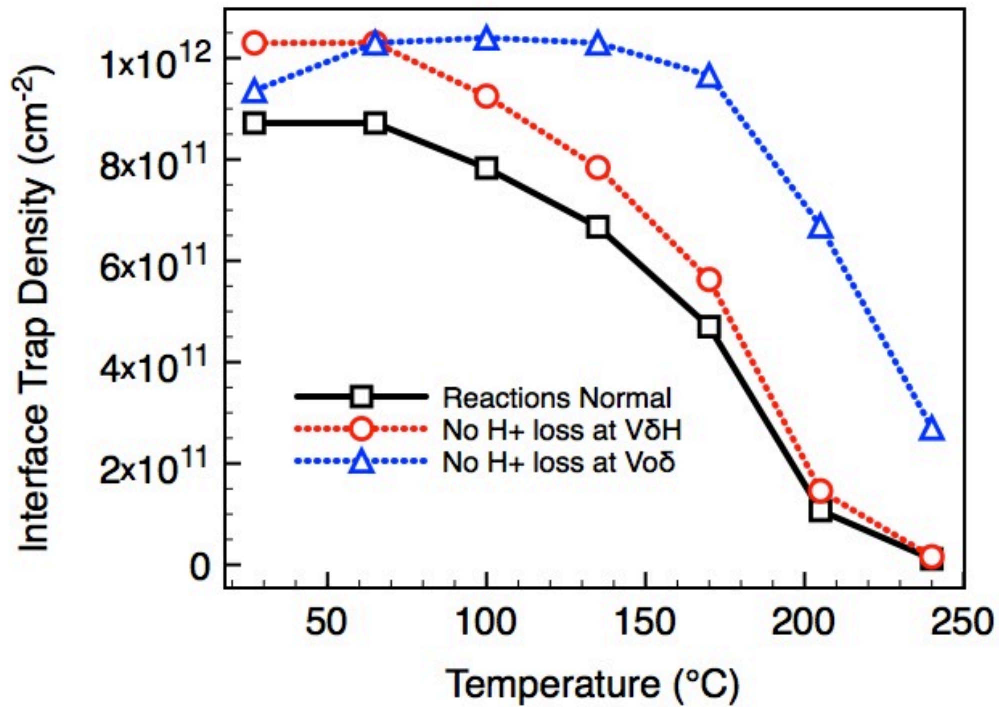

Fig. 5.6. Simulated interface-trap buildup versus temperature with proton capture at $V_{o\delta}$ defects suppressed (dashed blue line), defect-mediated dimerization at $V_{\delta}H$ defects suppressed (dashed red line), and with normal reactions (solid black line) with the H_2 concentration at 5×10^{21} cm^{-3}.

Elevated Temperature Irradiation Testing

These proton loss and passivation reactions are important to consider when evaluating accelerated testing methods. Elevated temperature irradiation was evaluated as a possible test to predict low dose rate degradation at higher dose rates, reducing the need for costly low dose rate tests [1], [2], [27], [47]-[50]. Experiments show that, while ETI can enhance degradation for parts exhibiting ELDRS as compared with room temperature irradiation at a moderate to high dose rate, the lower rate degradation is often significantly greater [2], [48], [51]. Fig. 5.7 shows results from [1] where excess base

current (correlated to interface-trap buildup) at 294 rad/s at elevated temperatures does not match the buildup seen at 0.001 rad/s at room temperature at 20 krad and 10 krad. Fig. 5.8 plots interface-trap buildup vs. temperature for 294 rad/s and 0.001 rad/s for 20 krad(SiO_2) total dose. While the same values of total dose and dose rates are used to facilitate comparison, these are general trends. 294 rad/s is representative of a high dose rate in this model and 0.001 rad/s represents a low dose rate; the specific value of total dose simply produces vertical shifts on the y-axis. These results demonstrate that while elevated temperatures at high dose rates can increase interface-trap buildup, the increase is limited and likely does not approach the levels seen at room temperature low dose rate irradiations. This is because proton loss processes limit the increased degradation at elevated temperatures. In parts with very high levels of H_2, at room temperature the interface-trap buildup at high dose rate is within a factor of two of the low dose rate results. At elevated temperatures and long irradiation times due to low dose rate, passivation reactions become significant at elevated temperatures. The hydrogen concentration affects the temperature at which passivation reactions become significant.

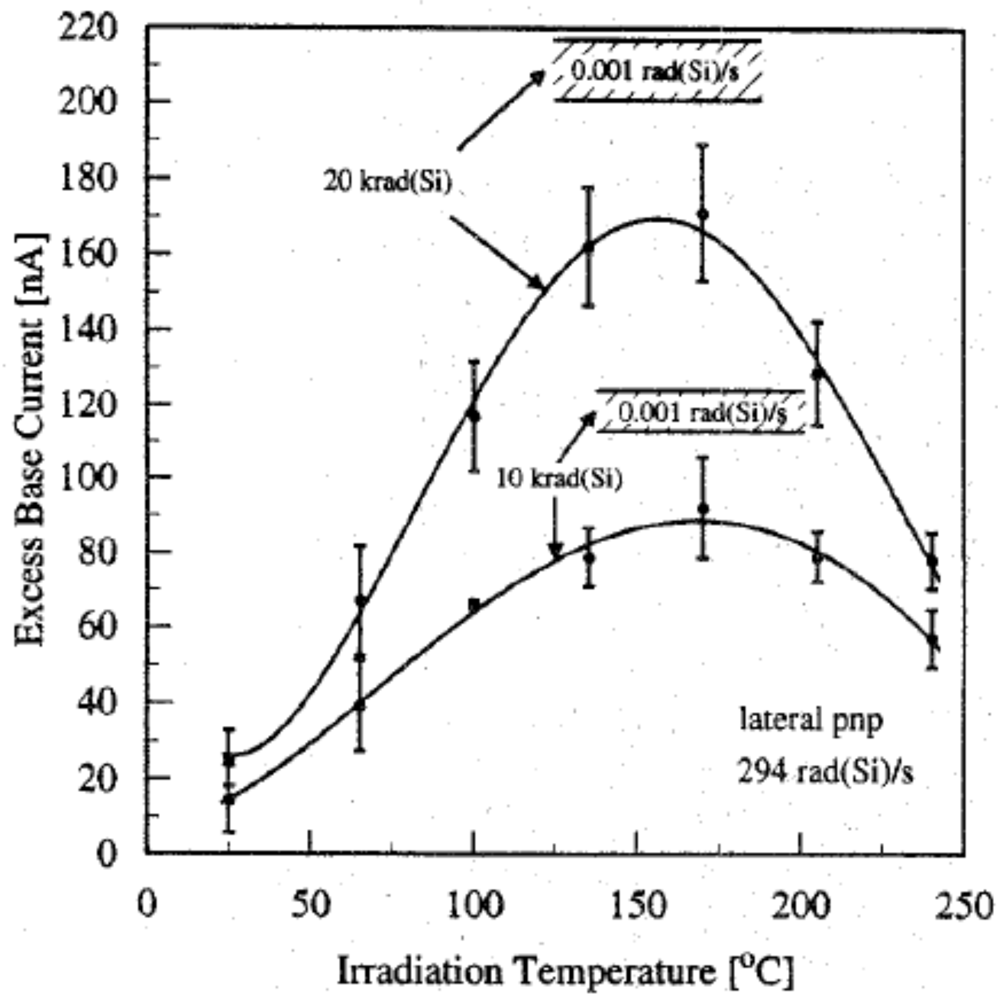

Fig. 5.7. Excess base current vs. temperature for pnp transistors irradiated with all terminals grounded at 294 rad/s at 10 krad(SiO_2) and 20 krad(SiO_2) with the room temperature results for a dose rate of 0.001 rad/s marked on the graph [1].

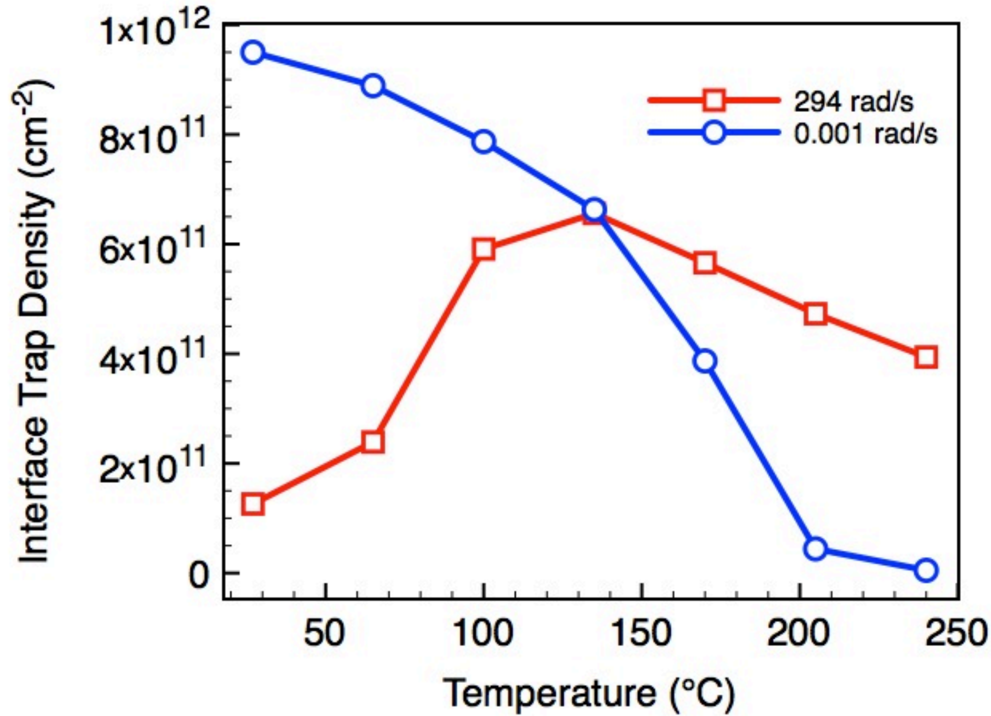

Fig. 5.8. Simulated interface-trap buildup vs. temperature at 294 rad/s and 0.001 rad/s at 20 krad(SiO_2). The H_2 concentration is 5×10^{17} cm^{-3}.

Another point to note is that measurements taken at elevated temperatures and high H_2 levels may be difficult to measure precisely. These factors together can make the passivation of interface traps occur on the timescale of the measurements. Fig. 5.9 shows the evolution of interface-trap density versus time after irradiation for a dose rate of 294 rad/s, at a temperature of 478 K, and with a H_2 concentration of 5×10^{21} cm^{-3}. The interface-trap density is reduced by half over the course of three minutes post irradiation. This helps explain why the model predicts higher degradation than the data in Fig. 5.2 since measurements from [1] were taken after cooling the part down from a given temperature. Higher temperatures and total doses enhance this effect, but the lower hydrogen concentrations reduce it.

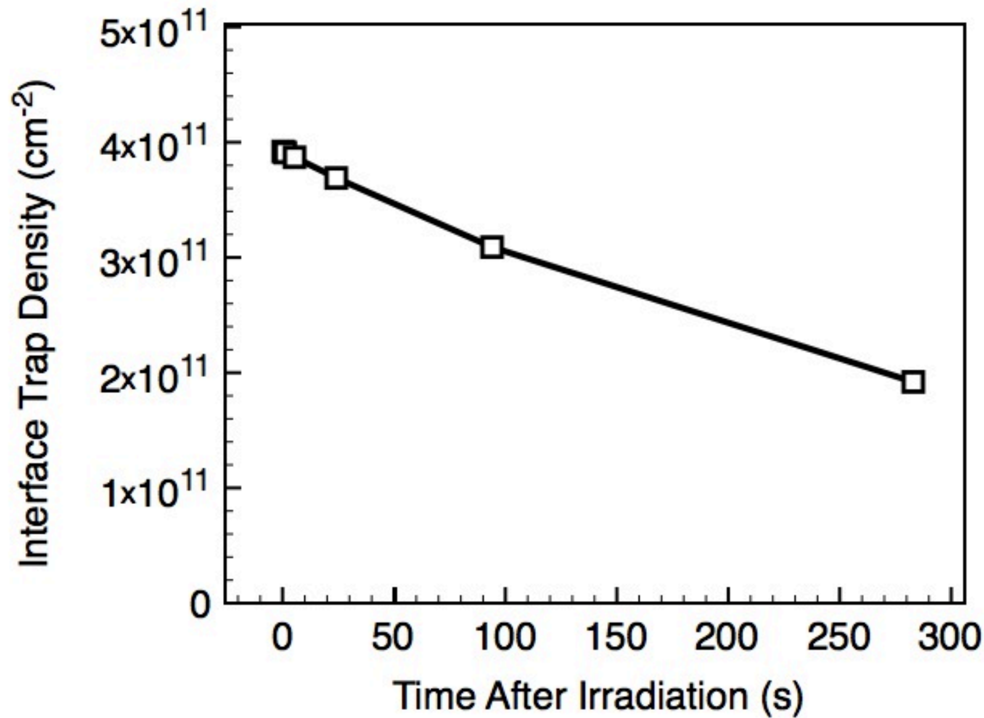

Fig. 5.9. Simulated interface-trap buildup vs. time after irradiation at 294 rad/s and 478 K with a H_2 concentration of 5×10^{21} cm^{-3}.

It is possible to match low dose rate degradation with higher dose rates in some cases [76]; however, using elevated temperature irradiation as a predictor can be inconsistent. Advance knowledge and characterization of potential parts is necessary to choose proper temperatures, dose rate, and total dose. Proton loss mechanisms do not become very effective until high concentrations of protons are produced, whether through a high concentration of molecular hydrogen or elevated temperatures. Elevated temperatures also have the dual effect of making the reaction rate coefficient more competitive. Picking a moderately elevated temperature helps maximize degradation. Additionally, choosing a dose rate lower than 294 rad(SiO_2)/s, but still higher than

something in the mrad(SiO_2)/s range can make the prediction more accurate. Lower total doses have also been found to be more predictive, likely because less interface-trap annealing occurs during the shortened irradiation time [8], [76]. The effect of total dose depends on the hydrogen concentration in the device as well. It may not be possible to predict low dose rate degradation at all, especially in parts that have very low concentrations of hydrogen since they will likely show very little enhanced degradation at elevated temperatures, as seen in Fig. 5.1.

Schematic Illustration

The reaction rate of proton loss reactions depends on both the reaction rate coefficient and the concentration of the reactants, VH defects and protons ($V_{o\delta}$ defects have a large enough concentration not to be limiting), and their low concentration can limit these reactions, especially at lower temperatures. However, the concentration of both protons and defects change with temperature. The progression from room temperature irradiation to enhanced interface-trap buildup to the saturation of interface-trap buildup is illustrated schematically in Fig. 5.10. VH_2 and $V_{o\gamma}$ are both sources of protons and are both represented as red dots to reduce clutter in the figure. $V_{o\delta}$ defects are represented as purple dots and are potential sites for proton trapping. VH defects are represented as green dots and are potential sites for hydrogen dimerization. In Fig. 5.10(a) the oxide is irradiated at room temperature. Protons are released by holes throughout the oxide and transport to the interface. The rate of proton capture by any type of defect is very low because the reaction rate coefficient, VH concentration, and proton concentration are all relatively low. The protons depassivate a portion of the Si-H bonds

to create interface traps. In Fig. 5.10(b) the oxide is irradiated at a moderately elevated temperature. The reaction rate coefficient for proton release increases and more protons are present in the oxide. They transport rapidly and buildup near the interface leading to increased interface-trap formation. The increases in temperature, reaction rate coefficients, VH concentration, and proton concentration are not large enough to cause the proton loss reactions to consume a significant portion of the protons near the interface. In Fig. 5.10(c) the oxide is irradiated at a temperature high enough to cause saturation of the interface-trap buildup. The increase in temperature causes a further increase in the reaction rate coefficient for proton loss reactions, the concentration of VH defects, and the concentration of protons. This results in a significant portion of the protons being trapped at $V_{o\delta}$ and VH defects, instead of depassivating Si-H bonds at the interface, suppressing interface-trap buildup.

Another factor that may play a role is that the interface-trap buildup at this point is relatively large. This leads to an increased reverse reaction rate for interface-trap creation, although this is a secondary effect compared to proton availability. While the reduction in proton concentration can limit the buildup of interface traps, the actual reductions in interface-trap density seen at very high temperatures likely are also enhanced by continued annealing processes (in the absence of additional proton generation) that inevitably occur while the parts are cooling down to be measured. If it were possible for the molecular hydrogen produced by the dimerization reaction to remain near the interface, this would also increase interface-trap annealing. However, at high temperatures H_2 diffuses quickly, limiting the additional amount of H_2 beyond the background concentration that is available for the passivation process.

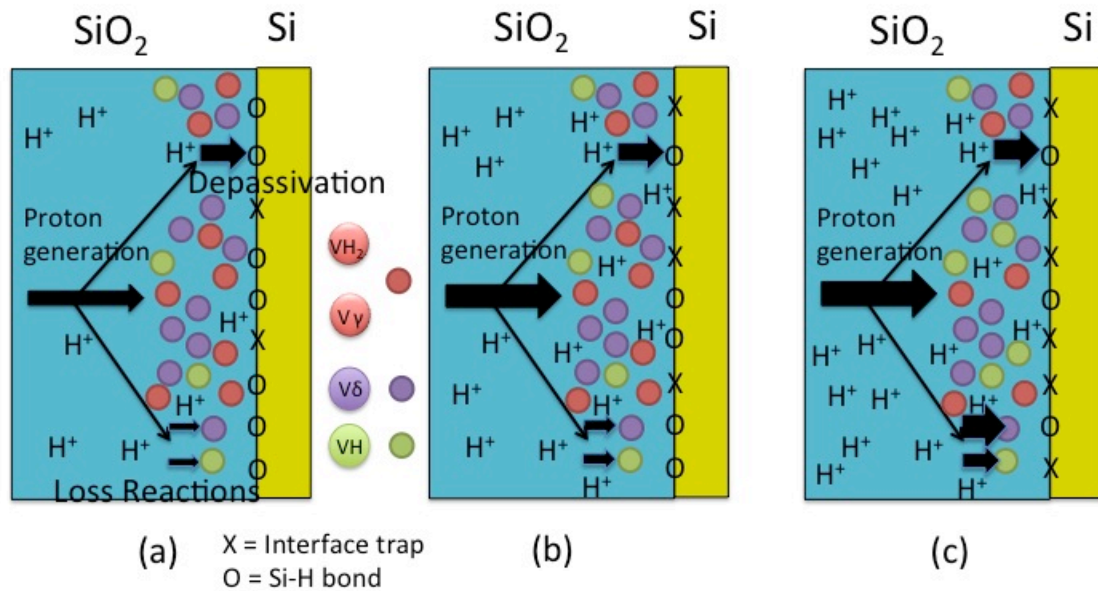

Fig. 5.10. Proton transport and interactions at or near the interface for room temperature and elevated temperature. H^+ is a proton, VH is a hydrogenated oxygen vacancy, VH_2 is a doubly hydrogenated oxygen vacancy, $V_{o\delta}$ is a dimer precursor oxygen vacancy, $V_{o\gamma}$ is a puckered precursor oxygen vacancy, O is a Si-H bond, X is an interface trap, and the size of the arrows are a rough approximation of the magnitudes of the reaction rate or speed of transport. (a) Oxide conditions at room temperature. (b) Oxide conditions at moderate temperature. (c) Oxide conditions at elevated temperatures.

CHAPTER VI

SUMMARY AND CONCLUSIONS

The buildup and annealing of radiation-induced interface traps is a significant issue for electronics in space that can be affected by many factors. The mechanisms that determine the extent of interface-trap buildup have been examined using the results of first principles physics calculations, an analytical model, and numerical simulations.

The numerical simulations are implemented based on physical parameters with a robust set of reactions to create a more realistic model than previously attempted. The defects in this model are identified by physics calculations to be present in significant concentrations in device quality oxides. Six different defects are considered in this model, including dimer and puckered versions of oxygen vacancies, singly hydrogenated oxygen vacancies, and doubly hydrogenated oxygen vacancies. Reactions were implemented in more fundamental terms than previously, including intermediate steps for every reaction. Including the intermediate step provides a more physical description because when a species is trapped at a defect there are multiple reaction pathways that can occur and each can have a different energy barrier. For example, when a hole is captured at a VH_2 defect, that defect becomes positively charged and a VH_2^+ defect is created. There are a number of reactions that may happen. The complex can release a proton, an H_2 molecule, capture an electron, or the hole may simply detrap. Which reaction happens is determined by the reaction rate for each potential reaction, which is calculated based on factors including the energy barrier and the concentrations of the products and reactants for each reaction.

The reaction rates and the transport parameters also contain temperature-dependent terms that change with the simulation temperature. The result is a detailed model that describes interface-trap buildup due to hydrogen interactions in silicon dioxide based on physical quantities provided by first principles physics calculations and data from the literature.

Proton generation that leads to interface-trap buildup is primarily due to interactions of positively charged oxygen vacancies in the puckered configuration with molecular hydrogen and the release of hydrogen already present in doubly hydrogenated oxygen vacancies via holes. Hydrogenated vacancies are created in the oxide during high temperature processing steps. The mechanisms identified are likely responsible for interface-trap buildup and annealing at varying temperatures, dose rates, H_2 concentrations, and total doses. At low levels of H_2, proton generation depends on hydrogenated vacancies, but as the H_2 concentration increases, the primary source of protons becomes H_2 dissociation at $V_{o\gamma}$ defects. Protons can be trapped at $V_{o\delta}$ and $V_{\delta}H$ defects, limiting proton supply near the interface and as a result, interface-trap formation. The effectiveness of this mechanism depends on temperature and proton concentration. At high levels of H_2, and thus, proton concentration, this can be significant at room temperature. As H_2 concentration decreases, proton loss at defects becomes significant with increasing temperature. At low dose rates, proton concentrations are lower, so proton loss reactions have little effect. As temperature and H_2 levels increase, the radiation response is dominated by interface-trap passivation, which occurs on the timescale of low dose rate irradiation. At elevated temperatures and H_2 levels, interface traps are passivated by hydrogen on the order of minutes after irradiation. This implies that accelerated tests involving high temperature irradiation are not an accurate

comparison to low dose rate irradiation since there are different mechanisms limiting interface-trap buildup. It may be possible to identify a temperature, dose rate, and total dose that is similar to low dose rate degradation, but extensive advance characterization is necessary since the mechanisms are not the same.

The research presented here accounts physically for general trends in temperature and dose rate behavior that have been seen in experimental data, but previously were not well understood. Understanding the mechanisms behind interface-trap buildup and annealing is critical for evaluating the radiation hardness of parts that operate at these conditions in space, and provides a better assessment of accelerated hardness assurance methods. ETI accelerates reactions and charge movement, which will increase interface-trap buildup. However, the increased proton concentration and changes in reaction rate coefficients create favorable conditions for proton loss mechanisms, opposing the increase in interface-trap concentration. Elevated temperatures also accelerate the passivation of interface traps via molecular hydrogen. This illustrates the need to carefully select the conditions for testing at elevated temperatures. Choosing a moderate temperature can maximize the buildup of interface traps without proton losses becoming significant. Minimizing the irradiation time through the choice of total dose and dose rate can prevent significant reductions in interface-trap density due to passivation reactions at the interface. The concentration of molecular hydrogen in the oxide is an extremely important variable and must be considered when performing ETI. If parts contain high concentrations of molecular hydrogen (due to a type of passivation for example), the effects of passivation appear at lower temperatures, as seen in Fig. 5.1. ETI becomes less effective as H_2 concentration increases; in fact for high levels of H_2 the highest

degradation occurs near room temperature. However, this degradation is not necessarily equal to low dose rate degradation and screening methods using exposure to excess H_2 need to be characterized in advance. While high concentrations of H_2 can cause ETI to be ineffective at increasing interface-trap buildup, parts that are manufactured in a way that minimizes hydrogen exposure will also see little effect from ETI. This is due to proton production through H_2 dissociation having a stronger temperature response than proton release via holes. When H_2 is not present in significant concentrations, elevated temperatures do not increase interface-trap buildup noticeable compared to mid to high levels of H_2. This is an important testing consideration if parts may be exposed to hydrogen later during their lifetime. As temperature effects on radiation response are more clearly understood, expected temperature profiles for parts to be exposed to radiation environments can be used to better predict degradation under a variety of conditions.

REFERENCES

[1] S. C. Witczak, R. D. Schrimpf, K. F. Galloway, D. M. Fleetwood, R. L. Pease, J. M. Puhl, D. M. Schmidt, W. E. Combs, and J. S. Suehle, "Accelerated tests for simulating low dose rate gain degradation of lateral and substrate pnp bipolar junction transistors," *IEEE Trans. Nucl. Sci.*, vol. 43, no. 6, pp. 3151–3160, Dec. 1996.

[2] R. L. Pease, L. M. Cohn, D. M. Fleetwood, M. A. Gehlhausen, T. L. Turflinger, D. R. Brown, and A. H. Johnston, "A proposed hardness assurance test methodology for bipolar linear circuits and devices in a space ionizing radiation environment," *IEEE Trans. Nucl. Sci.*, vol. 44, no. 6, pp. 1981–1988, Dec. 1997.

[3] R. L. Pease, G. W. Dunham, J. E. Seiler, D. G. Platteter, and S. S. McClure, "Total dose and dose rate response of an AD590 temperature transducer," *IEEE Trans. Nucl. Sci.*, vol. 54, no. 4, pp. 1049–1054, Aug. 2007.

[4] X. J. Chen, H. J. Barnaby, B. Vermeire, K. Holbert, D. Wright, R. L. Pease, G. Dunham, D. G. Platteter, J. Seiler, S. McClure, and P. Adell, "Mechanisms of enhanced radiation-induced degradation due to excess molecular hydrogen in bipolar oxides," *IEEE Trans. Nucl. Sci.*, vol. 54, no. 6, pp. 1913–1919, Dec. 2007.

[5] X. J. Chen, H. J. Barnaby, B. Vermeire, K. E. Holbert, D. Wright, R. L. Pease, R. D. Schrimpf, D. M. Fleetwood, S. T. Pantelides, M. R. Shaneyfelt, and P. Adell, "Post-irradiation annealing mechanisms of defects generated in hydrogenated bipolar oxides," *IEEE Trans. Nucl. Sci.*, vol. 55, no. 6, pp. 3032–3038, Dec. 2008.

[6] M. R. Shaneyfelt, R. L. Pease, J. R. Schwank, M. C. Maher, G. L. Hash, D. M. Fleetwood, P. E. Dodd, C. A. Reber, S. C. Witczak, L. C. Riewe, H. P. Hjalmarson, J. C. Banks, B. L. Doyle, and J. A. Knapp, "Impact of passivation layers on enhanced low-dose-rate sensitivity and pre-irradiation elevated-temperature stress effects in bipolar linear ICs," *IEEE Trans. Nucl. Sci.*, vol. 49, no. 6, pp. 3171–3179, Dec. 2002.

[7] A. H. Johnston, G. M. Swift, and B. G. Rax, "Total dose effects in conventional bipolar transistors and linear integrated circuits," *IEEE Trans. Nucl. Sci.*, vol. 41, no. 6, pp. 2427–2436, Dec. 1994.

[8] R. L. Pease, R. D. Schrimpf, and D. M. Fleetwood, "ELDRS in bipolar linear circuits: A review," *IEEE Trans. Nucl. Sci*., vol. 56, no. 4, pp. 1894-1908, Dec. 2009.

[9] R. L. Pease, P. C. Adell, B. Rax, S. McClure, H. J. Barnaby, K. Kruckmeyer, and B. Triggs, "Evaluation of an accelerated ELDRS test using molecular hydrogen," *IEEE*

Trans. Nucl. Sci., vol. 57, no. 6, pp. 3419-3425, Dec. 2010.

[10] D. Chen, R. Pease, K. Kruckmeyer, J. Forney, A. Phan, M. Carts, S. Cox, S. Burns, R. Albarian, B. Holcombe, B. Little, J. Salzman, G. Chaumont, H. Duperray, A. Ouellet, S. Buchner, and K. LaBel, "Enhanced low dose rate sensitivity at ultra-low dose rates," *IEEE Trans. Nucl. Sci.*, vol. 58, no. 6, pp. 2983-2990, Dec. 2011.

[11] B. R. Tuttle, D. R. Hughart, R. D. Schrimpf, D. M. Fleetwood, and S. T. Pantelides, "Defect interactions of H_2 in SiO_2: Implications for ELDRS and latent interface trap buildup," *IEEE Trans. Nucl. Sci.*, vol. 57, no. 6, pp. 3046–3053, Dec. 2010.

[12] S. N. Rashkeev, C. R. Cirba, D. M. Fleetwood, R. D. Schrimpf, S. C. Witczak, A. Michez, and S. T. Pantelides, "Physical model for enhanced interface-trap formation at low dose rates," *IEEE Trans. Nucl. Sci.*, vol. 49, no. 6, pp. 2650-2655, Dec. 2002.

[13] H. P. Hjalmarson, R. L. Pease, S. C. Witczak, M. R. Shaneyfelt, J. R. Schwank, A. H. Edwards, C. E. Hembree, and T. R. Mattsson, "Mechanisms for radiation dose-rate sensitivity of bipolar transistors," *IEEE Trans. Nucl. Sci.*, vol. 50, no. 6, pp. 1901–1909, Dec. 2003.

[14] F. B. McLean, "A framework for understanding radiation-induced interface states in SiO_2 MOS structures," *IEEE Trans. Nucl. Sci.*, vol. 27, no. 6, pp. 1651-1657, Dec. 1980.

[15] T. R. Oldham and F. B. McLean, "Total ionizing dose effects in MOS oxides and devices," *IEEE Trans. Nucl. Sci.*, vol. 50, no. 3, pp. 483–499, Jun. 2003.

[16] H. P. Hjalmarson, R. L. Pease, and R. A. B. Devine, "Calculations of radiation dose-rate sensitivity of bipolar transistors," *IEEE Trans. Nucl. Sci.*, vol. 55, no. 6, pp. 3009–3015, Dec. 2008.

[17] D. M. Fleetwood, R. D. Schrimpf, S. T. Pantelides, R. L. Pease, and G. W. Dunham, "Electron capture, hydrogen release, and enhanced gain degradation in linear bipolar devices," *IEEE Trans. Nucl. Sci.*, vol. 55, no. 6, pp. 2986–2991, Dec. 2008.

[18] D. R. Hughart, R. D. Schrimpf, D. M. Fleetwood, B. R. Tuttle, and S. T. Pantelides, "Mechanisms of interface trap buildup and annealing during elevated temperature irradiation," *IEEE Trans. Nucl. Sci.*, vol. 58, no. 6, pp. 2930-2936, Dec. 2011.

[19] R. L. Pease, P. C. Adell, B. G. Rax, X. J. Chen, H. J. Barnaby, K. E. Holbert, and H. P. Hjalmarson, "The effects of hydrogen on the enhanced low dose rate sensitivity (ELDRS) of bipolar linear circuits," *IEEE Trans. Nucl. Sci.*, vol. 55, no. 6, pp. 3169-3173, Dec. 2008.

[20] D. M. Fleetwood, L. C. Riewe, J. R. Schwank, S. C. Witczak, and R. D. Schrimpf, "Radiation effects at low electric fields in thermal, SIMOX, and bipolar-base

oxides," *IEEE Trans. Nucl. Sci.*, vol. 43, no. 6, pp. 2537–2546, Dec. 1996.

[21] S. C. Witczak, R. C. Lacoe, D. C. Mayer, D. M. Fleetwood, R. D. Schrimpf, and K. F. Galloway, "Space charge limited degradation of bipolar oxides at low electric fields," *IEEE Trans. Nucl. Sci.*, vol. 45, no. 6, pp. 2339–2351, Dec. 1998.

[22] L. Tsetseris, R. D. Schrimpf, D. M. Fleetwood, R. L. Pease, and S. T. Pantelides, "Common origin for enhanced-low-dose Rate Sensitivity and bias temperature instability under negative bias," *IEEE Trans. Nucl. Sci.*, vol. 52, no. 6, pp. 2265-2271, Dec. 2005.

[23] R. D. Schrimpf, "Physics and hardness assurance for bipolar technologies," Short course, section IV, NSREC 2001.

[24] D. M. Fleetwood and H. A. Eisen, "Total-dose radiation hardness assurance," *IEEE Trans. Nucl. Sci.*, vol. 50, no. 6, pp. 552-564, Dec. 2003.

[25] R. L. Pease, "Total ionizing dose effects in bipolar devices and circuits," *IEEE Trans. Nucl. Sci.*, vol. 50, no. 6, pp. 539-551, June 2003.

[26] R. L. Pease, D. G. Platteter, G. W. Dunham, J. E. Seiler, H. J. Barnaby, R. D. Schrimpf, M. R. Shaneyfelt, M. C. Maher, and R. N. Nowlin, "Characterization of enhanced low dose rate sensitivity (ELDRS) effects using gated lateral PNP transistor structures," *IEEE Trans. Nucl. Sci.*, vol. 51, no. 6, pp. 3773-3780, Dec. 2004.

[27] D. M. Fleetwood, S. L. Kosier, R. N. Nowlin, R. D. Schrimpf, R. A. Reber, Jr., M. Delaus, P. S. Winokur, A. Wei, W. E. Combs, and R. L. Pease, "Physical mechanisms contributing to enhanced bipolar gain degradation at low dose rates," *IEEE Trans. Nucl. Sci.*, vol. 41, no. 6, pp. 1871–1883, Dec. 1994.

[28] R. J. Graves, C. R. Cirba, R. D. Schrimpf, R. J. Milanowski, A. Michez, D. M. Fleetwood, S. C. Witczak, and F. Saigne, "Modeling low-dose-rate effects in irradiated bipolar-base oxides," *IEEE Trans. Nucl. Sci.*, vol. 45, no. 6, pp. 2352-2360, Dec. 1998.

[29] J. Boch, F. Saigne, R. D. Schrimpf, J.-R. Vaille, L. Dusseau, and E. Lorfevre, "Physical model for the low-dose-rate effect in bipolar devices," *IEEE Trans. Nucl. Sci.*, vol. 53, no. 6, pp. 3655-3660, Dec. 2006.

[30] M. R. Shaneyfelt, J. R. Schwank, S. C. Witczak, D. M. Fleetwood, R. L. Pease, P. S. Winokur, L. C. Riewe, and G. L. Hash, "Thermal-stress effects and enhanced low dose rate sensitivity in linear bipolar ICs," *IEEE Trans. Nucl. Sci.*, vol. 47, no. 6, pp. 2539-2545, Dec. 2000.

[31] P. M. Lenahan and P. V. Dressendorfer, "Radiation-induced paramagnetic defects in

MOS structures," *IEEE Trans. Nucl. Sci.*, vol. 29, no. 6, pp. 1459-1461, Dec. 1982.

[32] P. M. Lenahan and P. V. Dressendorfer, "Microstructural variations in radiation hard and soft oxides observed through electron spin resonance," *IEEE Trans. Nucl. Sci.*, vol. 30, no. 6, pp. 4602-4604, Dec. 1983.

[33] P. M. Lenahan and P. V. Dressendorfer, "Hole traps and trivalent silicon centers in metal/oxide/silicon devices," *J. Appl. Phys.*, vol. 55, no. 10, pp. 3495-3499, 1984.

[34] H. S. Witham and P. M. Lenahan, "Nature of the E' deep hole trap in metal-oxide-semiconductor oxides," *Appl. Phys. Lett.*, vol. 51, no. 13, pp. 1007-1009, 1987.

[35] J. F. Conley, Jr., P. M. Lenahan, H. L. Evans, R. K. Lowry, and T. J. Morthorst, "Observation and electronic characterization of two E' center charge traps in conventionally processed thermal SiO_2 on Si," *Appl. Phys. Lett.*, vol. 65, no. 18, pp. 2281-2283, 1994.

[36] C. J. Nicklaw, Z. Y. Lu, D. M. Fleetwood, R. D. Schrimpf, and S. T. Pantelides, "The structure, properties, and dynamics of oxygen vacancies in amorphous SiO_2," *IEEE Trans. Nucl. Sci.*, vol. 49, no. 6, pp. 2667–2673, Dec. 2002.

[37] S. N. Rashkeev, D. M. Fleetwood, R. D. Schrimpf, and S. T. Pantelides, "Effects of hydrogen motion on interface trap formation and annealing," *IEEE Trans. Nucl. Sci.*, vol. 51, no. 6, pp. 3158–3165, Dec. 2004.

[38] I. G. Batyrev, D. Hughart, R. Durand, M. Bounasser, B. R. Tuttle, D. M. Fleetwood, R. D. Schrimpf, S. N. Rashkeev, G. W. Dunham, M. Law, and S. T. Pantelides, "Effects of hydrogen on the radiation response of bipolar transistors: Experiment and modeling," *IEEE Trans. Nucl. Sci.*, vol. 55, no. 6, pp. 3039-3045, Dec. 2008.

[39] J. F. Conley, Jr. and P. M. Lenahan, "Molecular hydrogen, E' center hole traps, and radiation induced interface traps in MOS devices," *IEEE Trans. Nucl. Sci.*, vol. 40, no. 6, pp. 1335-1340, Dec. 1993.

[40] J. F. Conley, Jr. and P. M. Lenahan, "Room temperature reactions involving silicon dangling bond centers and molecular hydrogen in amorphous SiO_2 thin films on silicon," *Appl. Phys. Lett.*, vol. 62, no. 1, pp. 40-42, 1993.

[41] R. M. van Ginhoven, H. P. Hjalmarson, A. H. Edwards, and B. R. Tuttle, "Hydrogen release in SiO_2: Source sites and release mechanisms," *Nucl. Instrum. Methods Phys. Res. B, Beam Interact. Mater. At.*, vol. 250, pp. 274-278, 2006.

[42] X. J. Chen, H. J. Barnaby, P. Adell, R. L. Pease, B. Vermeire, and K. E. Holbert, "Modeling the dose rate response and the effects of hydrogen in bipolar technologies," *IEEE Trans. Nucl. Sci.*, vol. 56, no. 6, pp. 3196-3202, Dec. 2009.

[43] N. L. Rowsey, M. E. Law, R. D. Schrimpf, D. M. Fleetwood, B. R. Tuttle, and S. T. Pantelides, “A quantitative model for ELDRS and H_2 degradation effects in irradiated oxides based on first principles calculations,” *IEEE Trans. Nucl. Sci.*, vol. 58, no. 6, pp. 2937-2944, Dec. 2011.

[44] R. E. Stahlbush, A. H. Edwards, D. L. Griscom, and B. J. Mrstik, “Post-irradiation cracking of H_2 and formation of interface states in irradiated metal-oxide-semiconductor field effect transistors,” *J. Appl. Phys.*, vol. 73, no. 2, pp. 658–667, 1993.

[45] M. Vitiello, N. Lopez, F. Illas, and G. Pacchioni, “H_2 cracking at SiO_2 defect centers,” *J. Phys. Chem. A*, vol. 104, no. 20, pp. 4674–4684, 2000.

[46] R. M. van Ginhoven, H. P. Hjalmarson, A. H. Edwards, and B. R. Tuttle, “Hydrogen release in SiO_2 : Source sites and release mechanisms,” *Nucl. Instrum. Methods Phys. Res. B, Beam Interact. Mater. At.*, vol. 250, pp. 274–278, 2006.

[47] R. D. Schrimpf, R. J. Graves, D. M. Schmidt, D. M. Fleetwood, R. L. Pease, W. E. Combs, and M. Delaus, “Hardness-assurance issues for lateral PNP bipolar junction transistors,” *IEEE Trans. Nucl. Sci.*, vol. 42, no. 6, pp. 1641–1649, Dec. 1995.

[48] R. Nowlin, D. M. Fleetwood, and R. D. Schrimpf, “Saturation of the dose-rate response of bipolar transistors below 10 rad(SiO_2)/s: Implications for hardness assurance,” *IEEE Trans. Nucl. Sci.*, vol. 41, no. 6, pp. 2637–2641, Dec. 1994.

[49] R. D. Schrimpf, “Recent advances in understanding total-dose effects in bipolar transistors,” *IEEE Trans. Nucl. Sci.*, vol. 43, no. 3, pp. 787–796, June 1996.

[50] S. C. Witczak, R. D. Schrimpf, D. M. Fleetwood, K. F. Galloway, R. C. Lacoe, D. C. Mayer, J. M. Puhl, R. L. Pease, and J. S. Suehle, “Hardness assurance testing of bipolar junction transistors at elevated irradiation temperatures,” *IEEE Trans. Nucl. Sci.*, vol. 44, no. 6, pp. 1989–2000, Dec. 1997.

[51] R. L. Pease, M. Gehlhausen, J. Krieg, J. Titus, T. Turflinger, D. Emily, and L. Cohn, “Evaluation of proposed hardness assurance method for bipolar linear circuits with enhanced low dose rate sensitivity (ELDRS),” *IEEE Trans. Nucl. Sci.*, vol. 45, no. 6, pp. 2665–2672, Dec. 1998.

[52] M. R. Shaneyfelt, J. R. Schwank, D. M. Fleetwood, R. L. Pease, J. A. Felix, P. E. Dodd, and M. C. Maher, “Annealing behavior of linear bipolar devices with enhanced low-dose-rate sensitivity,” *IEEE Trans. Nucl. Sci.*, vol. 51, no. 6, pp. 3172-3177, Dec. 2004.

[53] P. V. Sushko, S. Mukhopadhyay, A. S. Mysovsky, V. B. Sulimov, A. Taga, and A. L. Shluger, “Structure and properties of defects in amorphous silica: New insights from embedded cluster calculations,” *J. Phys., Condens. Matter.*, vol. 17, no. 21, pp.

S2115–S2140, 2005.

[54] S. Girard, N. Richard, Y. Ouerdane, G. Origlio, A. Boukenter, L. Martin-Samos, P. Paillet, J.-P. Meunier, J. Baggio, M. Cannas, and R. Boscaino, “Radiation effects on silica-based preforms and optical fibers-II: Coupling *ab initio* simulations and experiments,” *IEEE Trans. Nucl. Sci.*, vol. 55, no. 6, pp. 3508–3514, Dec. 2008.

[55] Z. Y. Lu, C. J. Nicklaw, D. M. Fleetwood, R. D. Schrimpf, and S. T. Pantelides, “Structure, properties, and dynamics of oxygen vacancies in amorphous SiO_2 ,” *Phys. Rev. Lett. Article no. 285505*, vol. 89, 2002.

[56] F. J. Feigl, W. B. Fowler, and K. L. Yip, “Oxygen vacancy model for the E'_1 center in SiO_2 ,” *Solid State Commun.*, vol. 14, pp. 225–234, 1974.

[57] W. L. Warren, M. R. Shaneyfelt, J. R. Schwank, D. M. Fleetwood, P. S. Winokur, R. A. B. Devine, W. P. Maszara, and J. B. McKitterick, "Paramagnetic defect centers in irradiated BESOI and SIMOX buried oxides," *IEEE Trans. Nucl. Sci.*, vol. 40, no. 6, pp. 1755-1764, Dec. 1993.

[58] J. F. Conley, Jr. and P. M. Lenahan, “Electron spin resonance analysis of EP center interactions with H_2: Evidence for a localized EP center structure,” *IEEE Trans. Nucl. Sci.*, vol. 42, no. 6, pp. 1740–1743, Dec. 1995.

[59] G. Buscarino, S. Agnello, and F. M. Gelardi, “Delocalized nature of the E'_δ center in amorphous silicon dioxide,” *Phys. Rev. Lett.*, vol. 94, 2005, Article no. 125501.

[60] B. Tuttle and S. T. Pantelides, “Vacancy-related defects and the E'_δ center in amorphous silicon dioxide: Density functional calculations,” *Phys. Rev. B*, vol. 79, 2009, Article no. 115206.

[61] J. Godet and A. Pasquarello, “Proton diffusion in amorphous silica,” *Phys. Rev. Lett.*, vol. 97, 2006, Article no. 155901.

[62] D. R. Ball, R. D. Schrimpf, and H. J. Barnaby, “Separation of ionization and displacement damage using gate-controlled lateral PNP bipolar transistors,” *IEEE Trans. Nucl. Sci.*, vol. 49, no. 6, pp. 3185–3190, Dec. 2002.

[63] W. L. Warren, D. M. Fleetwood, M. R. Shaneyfelt, J. R. Schwank, P. S. Winokur, R. A. B. Devine, and D. Mathiot, “Links between oxide, interface, and border traps in high-temperature annealed Si/SiO2 systems,” *Appl. Phys. Lett.*, vol. 64, no. 25, pp. 3452–3454, 1994.

[64] K. Vanheusden, W. L. Warren, R. A. B. Devine, D. M. Fleetwood, J. R. Schwank, M. R. Shaneyfelt, P. S. Winokur, and Z. J. Lemnios, "Non-volatile memory device based on mobile protons in SiO_2 thin films," *Nature*, vol. 386 (6625), pp. 587-589, April 1997.

[65] P. E. Bunson, M. Di Ventra, S. T. Pantelides, R. D. Schrimpf, and K. F. Galloway, "*Ab initio* calculations of H^+ energetics in SiO_2: Implications for transport," *IEEE Trans. Nucl. Sci.*, vol. 46, no. 6, pp. 1568-1573, Dec. 1999.

[66] S. T. Pantelides, S. N. Rashkeev, R. Buczko, D. M. Fleetwood, and R. D. Schrimpf, "Reactions of hydrogen with Si-SiO_2 interfaces," *IEEE Trans. Nucl. Sci.*, vol. 47, no. 6, pp. 2262-2268, Dec. 2000.

[67] T. P. Ma and P. V. Dressendorfer, *Ionizing Radiation Effects in MOS Devices and Circuits*. New York: Wiley-Interscience, 1989.

[68] R. C. Hughes, "Time resolved hole transport in a-SiO_2," *Phys. Rev. B* **15**, 2012 (1977).

[69] J. R. Srour, S. Othmer, O. L. Curtis, Jr., and K. Y. Chiu, "Radiation induced charge transport and charge buildup in SiO_2 films at low temperatures," *IEEE Trans. Nucl. Sci.*, vol. 23, no. 6, pp. 1513-1519, Dec. 1976.

[70] M. E. Law and S. M. Cea, "Continuum based modeling of silicon integrated circuit processing: An object oriented approach," *Computational Materials Science*, vol. 12, no. 4, pp. 289-308, 1998.

[71] D. L. Scharfetter and H. K. Gummel, "Large-signal analysis of a silicon read diode oscillator," IEEE Trans. Electron Devices, vol. 16, no. 1, pp. 64–77, Jan. 1969.

[72] D. J. Cummings, M. E. Law, S. Cea, and T. Linton, "Comparison of discretization methods for device simulation," in International Conference on Simulation of Semiconductor Processes and Devices, 2009. SISPAD '09., Sep. 2009, pp. 1–4.

[73] D. M. Fleetwood, P. S. Winokur, M. R. Shaneyfelt, and L. C. Riewe, "Effects of isochronal annealing and irradiation temperature on radiation-induced trapped charge," *IEEE Trans. Nucl. Sci.*, vol. 45, no. 6, pp. 2366-2374, Dec. 1998.

[74] B. R. Tuttle, "Energetics and diffusion of hydrogen in SiO_2," *Phys. Rev. B* **61**, 4417 (2000).

[75] S. N. Rashkeev, R. D. Schrimpf, D. M. Fleetwood, and S. T. Pantelides, "Defect generation by hydrogen at the Si-SiO_2 interface," *Phys. Rev. Lett.*, **87**, 165506 (2001).

[76] T. Carriere, R. Ecoffet, and P. Poirot, "Evaluation of accelerated total dose testing of linear bipolar circuits," *IEEE Trans. Nucl. Sci.*, vol. 47, no. 6, pp. 2350-2357, Dec. 2000.